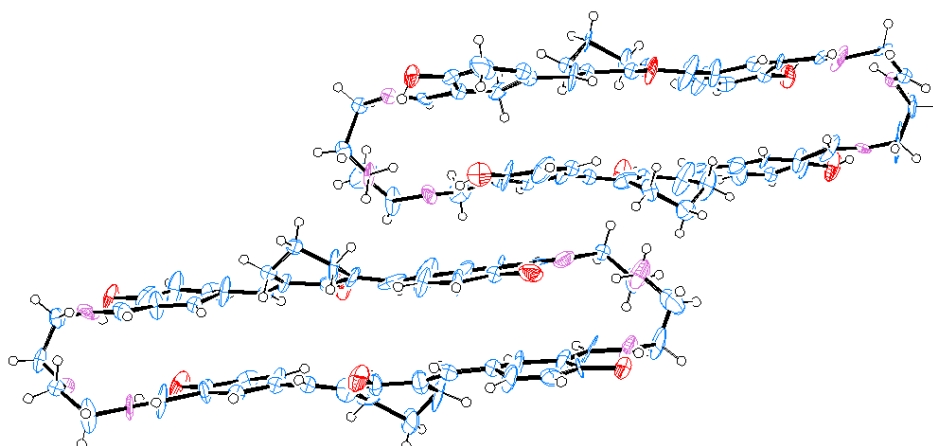
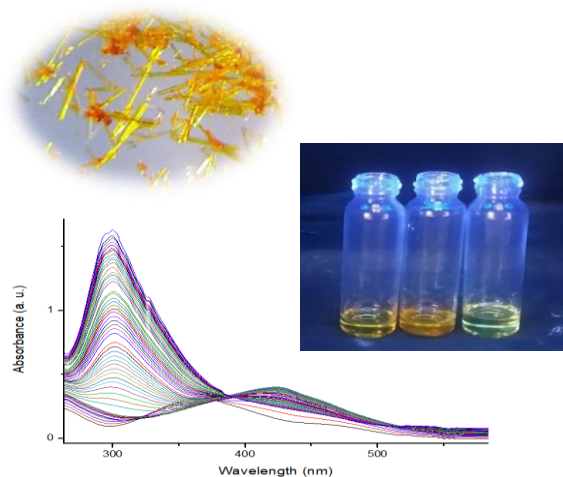


## Chapter 4

# Design and Synthesis of Curcuminoid based Gadolinium Corate and Supramolecular Vesicle for Development of Drug Delivery System

## Part-A

### Synthesis of Gd-Corate



---

#### 4.A.1. Introduction

Magnetic resonance imaging (MRI) is a highly effective medical diagnostic tool<sup>1</sup>, whose effectiveness is significantly enhanced by the utilization of exogenous contrast agents (CA)<sup>2,3</sup>. The two most widely used contrast agents are T1 (positive contrast agents) and T2 (negative contrast agents). T2 contrast agents are used to reduce the longitudinal relaxation time (spin lattice relaxation time) of protons, while T1 contrast agents are used for reducing the transverse or spin-spin relaxation time<sup>4</sup>. Superparamagnetic iron oxide nanoparticles are the most commonly studied T2 agent, while lanthanide ion-based CAs ( $Gd^{3+}$ ,  $Eu^{3+}$ ,  $Dy^{3+}$ ) are most commonly used T1 agent<sup>5,6</sup>.

Due to its unique magnetic characteristic, gadolinium ( $Gd^{3+}$ ) is the most often employed contrast agent in MRI<sup>7</sup>. This substance is employed in almost half of MRI scans<sup>8</sup> and aids in the greater visibility of tumours, blood vessels, inflammation, and infections in the targeted organs<sup>9</sup>. The free ions of gadolinium ( $Gd^{3+}$ ), are extremely poisonous and their build-up in the body causes biological toxicity<sup>10</sup>. Chelate ligand complexes, such Dotarem ( $Gd$ -DOTA), are utilised to lessen the toxicity of metal ions, but there are worries over the release of  $Gd^{3+}$  ions and their potentially detrimental effects.

For developing a carrier to coordinate the  $Gd^{3+}$  ion, creative and strategic ligand design is essential. The potential of a captive metal can be unlocked and its powers can completely be utilised by modifying and improving a ligand. If a metal complex is intended for its usage in a biological environment, the distribution, localization, and behaviour of the complex in a dynamic system are determined by the appropriate design of ligand motif<sup>11</sup>.

The 1, 4, 7, 10-tetraazacyclododecane-1, 4, 7, 10-tetraacetic acid ( $H_4$ DOTA) ligand is widely referred to as the "gold standard" in trivalent gadolinium chelation (figure 4.1). This ligand is composed of the macrocycle cyclen, which is N-functionalized with four pendant arms of acetic acid and is octadentate with four donor atoms of nitrogen and four donor atoms of oxygen.  $[Gd(OH_2)(DOTA)]$  is still the most thermodynamically stable gadolinium based contrasting agent (GBCA) in clinical use.  $H_4$ DOTA has therefore shown to be an appealing scaffold for modification because of its good chelating properties<sup>12</sup>.

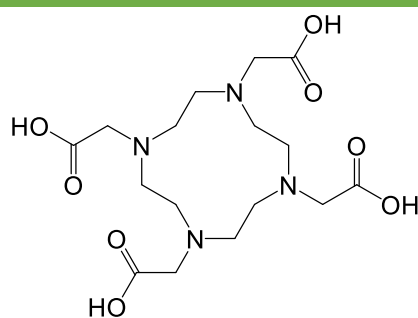


Figure. 4.1. General structure of 1, 4, 7, 10-tetraazacyclododecane-1, 4, 7, 10-tetraacetic acid (H<sub>4</sub>DOTA).

Xu et. al. effectively synthesised MTX-Gd, a novel stable and distinctive theranostic agent that was intended for use in the detection and treatment of cancer. By combining MTX and Gd through 1, 4, 7, 10-tetraazacyclododecane-1, 4, 7, 10-tetraacetic acid (Gd-DOTA), MTX-DOTA-Gd was created. The experiment revealed that MTX-DOTA-Gd has outstanding magnetic capacity, powerful anticancer properties, and good stability<sup>13</sup> (figure 4.2).

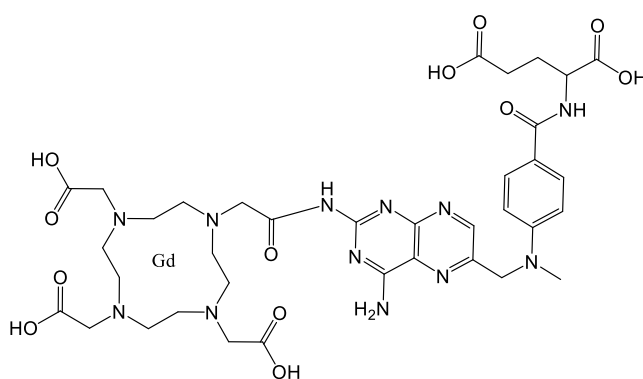


Figure. 4.2. Structure of MTX-DOTA-Gd synthesized by Xu et. al.

Using the DCC-NHS coupling process, Jeong et. al. created a novel CA from DOTA with primary amine modified lactobionic acid (Gd-DOTA-LAE). Comparing in vitro paramagnetic characteristics to traditional macrocyclic CA, they revealed a considerably improved T1 contrast effect. Additionally, 20 minutes after injection, Gd-DOTA-LAE demonstrated 29% greater contrast intensity at tumour sites compared to normal tissues. These findings confirm the clinical applicability of Gd-DOTA-LAE in MR imaging<sup>14</sup> (figure 4.3).

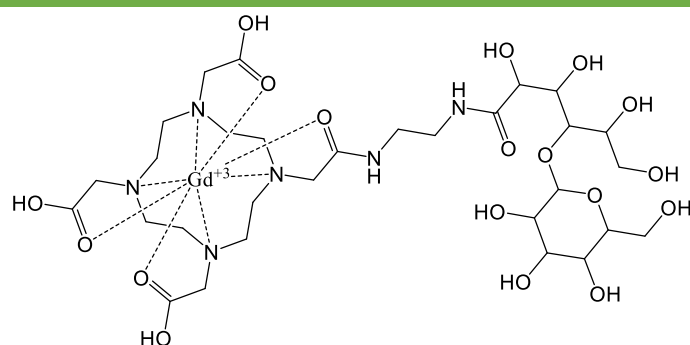


Figure. 4.3. Structure of Gd-DOTA-LAE synthesized by Jeong et.al.

In addition to study the effects of ultrasound/MR imaging on B16F10 melanoma cancer cells, Maghsoudinia et. al. evaluated the effect of Gd-DOTA/doxorubicin-loaded perfluorohexane nanodroplets as a theranostic nanodroplet for control released drug delivery. In order to synthesize nanodroplet (NDs) they homogenized the Gd-DOTA (Dotarem, 0.5 mmol/ml, 1 ml), and surfactant (Tween 20, 10 L) to the perfluorohexane solution with subsequent addition of alginate polysaccharide (1.5% w/v) and  $\text{CaCl}_2$  (0.2 w/v). The synthesised nanodroplets demonstrated ultrasound (US) and MRI guided drug release, and excellent *in vivo* and *in vitro* biocompatibility. Gd-DOTA/DOX@PFH NDs can act as US/MRI-guided drug delivery nanocarriers to increase the effectiveness of chemotherapy on melanoma cancer cells<sup>15</sup>.

Gallo et. al. created two novel peptide-Gd conjugates, DTPA(Gd)-PEG8-(FY)3 and DOTA(Gd)-PEG8-(FY) (figure 4.4). Both of these peptide conjugates can produce soft hydrogels. The high relaxivity value ( $12 \text{ mM}^{-1} \text{ s}^{-1}$  at 20 MHz) and extremely minimal *in vitro* cytotoxicity of these nanostructure showed their potential uses as supramolecular MRI diagnostic agents<sup>16</sup>.

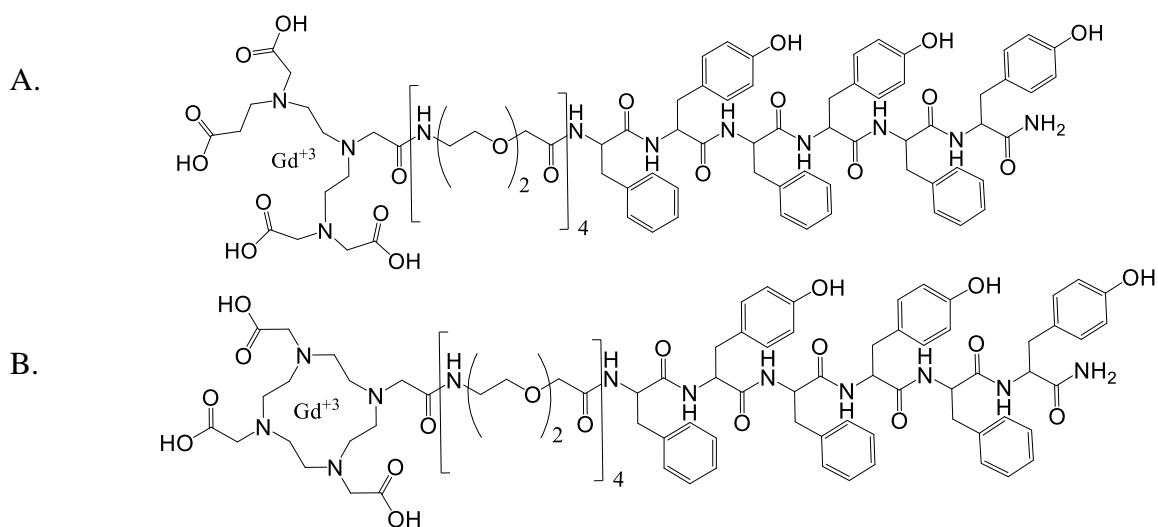


Figure. 4.4. Schematic representation of A.) DTPA(Gd)-PEG8-(FY)3, B.) DOTA(Gd)-PEG8-(FY)3.

---

A molecular theranostic prodrug created by Yang et. al. includes the anticancer drug camptothecin (CPT), the targeting agent biotin, and a modified gadolinium (III)-1, 4, 7, 10-tetraazacyclododecane-1, 4, 7, 10-tetraacetate (Gd-DOTA) complex. The newly discovered innovative theranostic prodrug demonstrated real-time monitoring by MRI, which offers superior spatial resolution and soft tissue contrast<sup>17</sup> (figure 4.5).

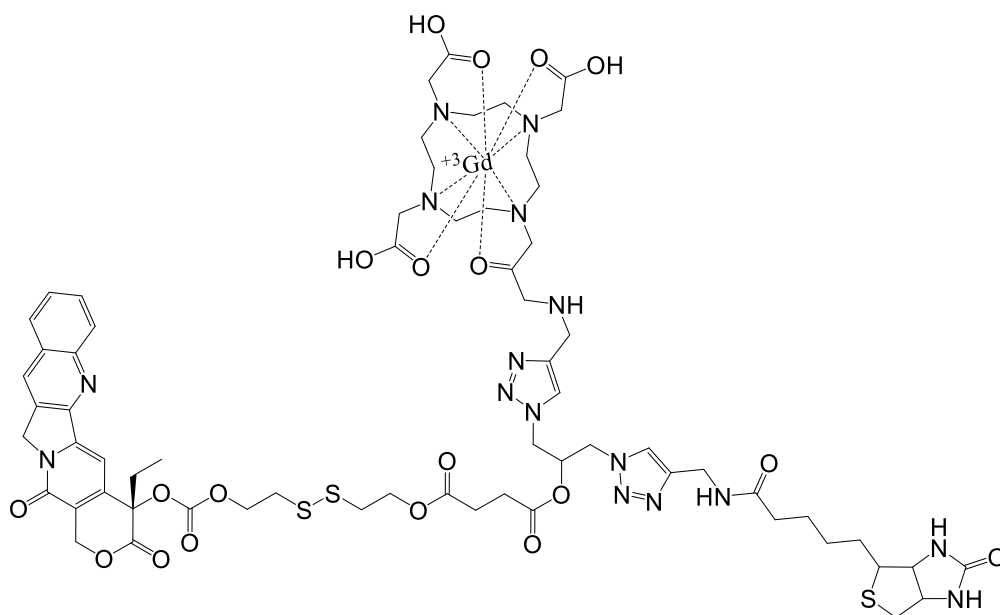


Figure. 4.5. A modified gadolinium (III)-1, 4, 7, 10-tetraazacyclododecane-1, 4, 7, 10-tetraacetate (Gd-DOTA) complex with anticancer drug camptothecin (CPT) and targeting agent biotin.

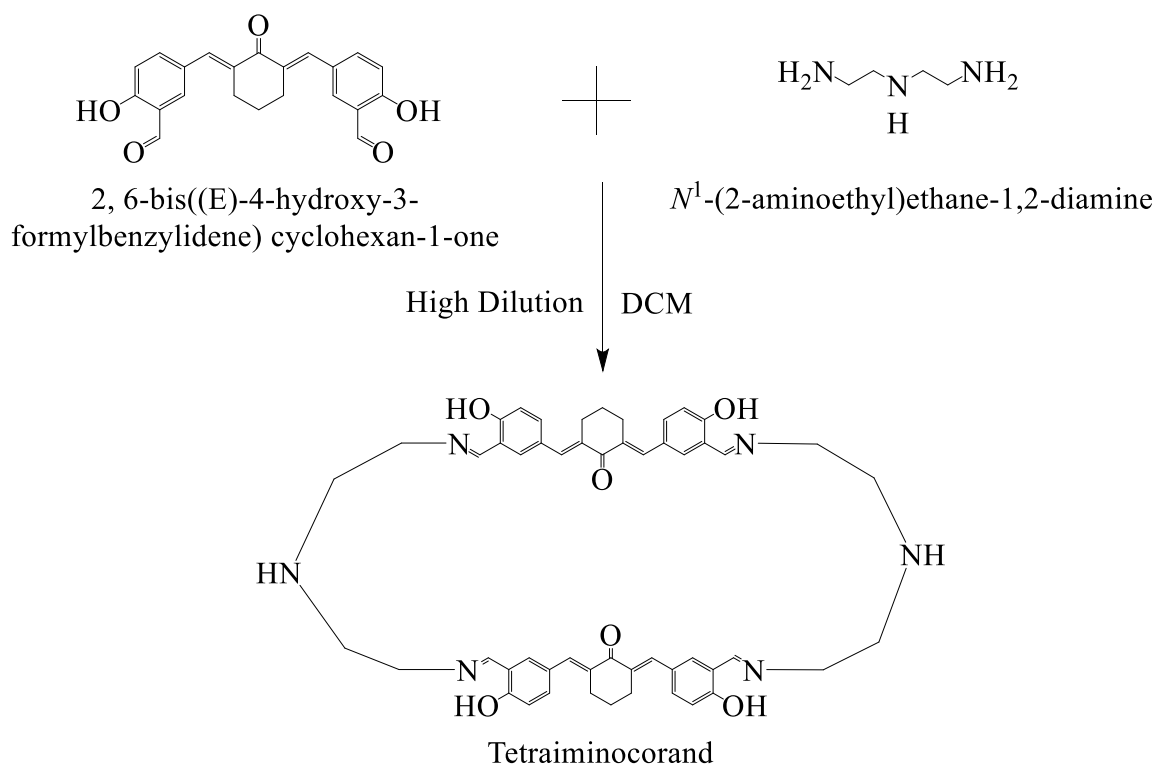
In the present work we developed a drug carrier with the chelating site for gadolinium to encapsulate it into the cavity which can be developed as MRI guided drug delivery system. The carrier was synthesized by using bis-aldehyde of cyclohexanone based curcuminoid and N<sup>1</sup>- (2-aminoethyl)ethane-1, 2-diamine.

## 4.A.2. Experimental Section

### 4.A.2.1. Materials

The chemicals and solvents used in the preparation of curcuminoid based tetraaminocorand were of analytical grade and purchased from Merck, Spectrochem, Loba chemicals, TCI and SRL. Chemicals were used without further purification.

### 4.A.2.2. Synthesis of tetraaminocorand



Scheme.4.1. Synthesis of tetraaminocorand.

2 L DCM was placed in a 5 L 3-necked round bottom flask equipped with 2 dropping funnels. One dropping funnel contained (1 g, 0.0027 moles) of bis-aldehyde dissolved in 750 ml of DCM and another dropping funnel contained (0.28 g, 0.0027 moles) of  $N^1$ -(2-aminoethyl)ethane-1, 2-diamine dissolved in 750 ml of DCM. Both solutions were added drop wise to mechanically stirred 2 L DCM over 7 to 8 hours. The reaction mixture was concentrated to 50 ml and chromatographed on silica gel column using DCM: MeOH gradient elution. The orange crystalline product was obtained.

**Yield:** 57 %

**M. P.:** 220 °C (degraded)

---

**FT-IR** (KBr disc,  $\text{cm}^{-1}$ ): 3418.93( $\nu_{\text{-OH}}$ ), 2923.28( $\nu_{\text{-CHas}}$ ), 2862.19( $\nu_{\text{-CHs}}$ ), 1635.38( $\nu_{\text{-C=N}}$ ), 1594.41( $\nu_{\text{-C=C}}$ ).

**$^1\text{H}$ NMR:** (400 MHz,  $\text{CDCl}_3$ ):  $\delta$  13.58 (1H, s), 8.19 (1H, s), 7.60 (1H, s), 7.42 (1H,  $J_1 = 8.4$  Hz,  $J_2 = 2.0$  Hz, dd), 6.93 (1H,  $J = 1.6$  Hz, d), 6.79 (1H,  $J = 8.8$  Hz, d), 3.73 (2H, s), 3.00 (2H, t), 2.72 (2H, t), 1.73-1.63 (1H, m).

**$^{13}\text{C}$ NMR:** (400 MHz,  $\text{CDCl}_3$ ):  $\delta$  188.45, 166.09, 162.09, 135.98, 135.03, 133.99, 133.87, 126.54, 117.75, 117.42, 58.96, 48.21, 28.55, 22.82.

**DEPT135 NMR:** (400 MHz,  $\text{CDCl}_3$ ):  $\delta$  166.11, 135.98, 135.03, 133.99, 117.42, 58.95, 48.22, 28.56, 22.83.

**HRMS:** 430.2131 [(M/2)+1] (Theoretical mass [(M/2)+1] = 430.2052).

#### **4.A.2.3. UV-VIS titration of Gadoliniumacetate and Flufenamic acid with Tetraiminocorand**

2 ml of  $1 \times 10^{-5}$  M solution of tetraiminocorand in DMSO was placed into cuvette.  $2 \times 10^{-3}$  M solution of gadoliniumacetate and flufenamic acid were prepared in DMSO. UV-Vis titrations were carried out by adding 1  $\mu\text{l}$ ,  $2 \times 10^{-3}$  M solution of gadoliniumacetate upto 1 equivalent of tetraiminocorand then further titrated this solution by adding 1  $\mu\text{l}$ ,  $2 \times 10^{-3}$  M flufenamic acid.

#### **4.A.2.4. Synthesis of Gadolinium corate and Encapsulation of Flufenamic acid**

Briefly, 1 ml methanolic solution of gadoliniumacetate (1.9 mg, 0.00582 mmol) was mixed with the 5 ml solution of corand (5 mg, 0.00582 mmol) in mixture of solvents DCM: methanol ::3:2. The resultant mixture was then sonicated and kneaded in dark condition. It was dried in dark to obtain a free flowing powder. 5 ml of DCM used to dissolve of 11.7 mg (0.0419 mmol) of flufenamic acid was further added to the 5 mg (0.00419 mmol) of Gd-corate in 5 ml mixture of solvents of DCM:methanol solution. The resultant formulation was kneaded and dried to obtain a free flowing powder.

#### **4.A.2.5. Calculation of Drug Loading (DL%) of Gd-corate and Encapsulation Efficiency (EE%) of Flufenamic acid**

The aqueous solution of 2.9 mg inclusion complex of in 2 ml conductivity water was prepared and placed into 0.1-0.5 kD MWCO, Float-A-Lyzer G2, CE, Dialysis Membrane device from Repligen (Spectrum Laboratories), Inc. and subjected to dialysis in 100 ml water for 24 hours at room temperature. The concentration of free drug was determined by withdrawal of 5 ml of release medium and measuring absorption on UV-Vis-spectrophotometer. Utilising an

---

ultraviolet detection wavelength of 287 nm, spectrophotometry was used to quantify the amount of drug contained in the inclusion complexes. The concentration of unbound drug was subtracted from the drug added to the carrier to determine the amount of drug loaded.

Using the following formulae<sup>18</sup>, the drug loading (DL) and entrapment efficiency (EE) were estimated in comparison to the standard curve:

$$DL (\%) = [(W_{\text{Flufenamic acid}} - W_{\text{Unbound Flufenamic acid}}) / W_{\text{Inclusion complex}}] \times 100$$

$$EE (\%) = [(W_{\text{Flufenamic acid}} - W_{\text{Unbound Flufenamic acid}}) / W_{\text{Flufenamic acid}}] \times 100$$

Where,

$W_{\text{Flufenamic acid}}$  = Weight of flufenamic acid in inclusion complex

$W_{\text{Unbound Flufenamic acid}}$  = Weight of unbound flufenamic acid released from inclusion complex

$W_{\text{Inclusion complex}}$  = Weight of inclusion complex

#### **4.A.2.6. Cumulative release profile of Flufenamic acid**

Dialysis bag method<sup>19</sup> was used to investigate the in vitro release profile of flufenamic acid at two different pH levels (7.4 and 5.5). Briefly, 0.1-0.5kD MWCO, Float-A-Lyzer G2, CE, Dialysis Membrane device from Repligen (Spectrum Laboratories), Inc. was used for dialysis. 2 mL aqueous solution of 1.8 mg of inclusion complex was used for an experiment. 100 ml of buffer at pH 5.5 and pH 7.4 were used as release medium. A predefined volume of the release medium (5 ml) was withdrawn at regular intervals, and an equal volume of freshly made buffer was then supplied to make up for this withdrawal. A UV-Visible spectrophotometer was used to determine the concentration of the drug released.

#### **4.A.2.7. Characterization Method**

FT-IR studies of all compounds were performed on Bruker Alpha FT-IR spectrometer in solid state as KBr pellets. UV-visible Spectrophotometer experiments were performed on Perkin Elmer Lambda 35 Spectrophotometer, Inc, MA, USA. NMR data was recorded on Bruker AVANCE, 400 MHz spectrometer in CDCl<sub>3</sub> and DMSO-d<sub>6</sub>, with TMS as internal standard. A Bruker APEX-II CCD was used to acquire diffraction data for all of the synthesized compounds using graphite monochromatic Mo K $\alpha$  radiation (0.71073). The Olex 2<sup>70</sup> software and the ShelXL<sup>71</sup> refinement package were used to solve and refine all structures. MERCURY was used to create the graphics (version 3.9). Direct approaches were used to solve all structures, which were then refined in a regular way. Non-hydrogen atoms were treated anisotropically in all circumstances.

---

### 4.A.3. Results and Discussion

The curcuminoid based tetraaminocorand was synthesized by high dilution approach. When it comes to the cyclization of tiny organic compounds, Paul Ruggli and Karl Ziegler originally proposed the high dilution principle, which states that low concentrations of the starting precursor favour cyclization over chain formation<sup>20</sup>. The excess solvent and low concentration of reactants helps in the formation of intramolecular cyclisation and avoid the polymer generation. A tetraaminocorand was synthesized from bis-aldehyde (synthesized in chapter 2) and N<sup>1</sup>- (2-aminoethyl)ethane-1, 2-diamine in excess of dichloromethane to achieve [2+2] cyclocondensed product (scheme 4.1) (figure 4.6).

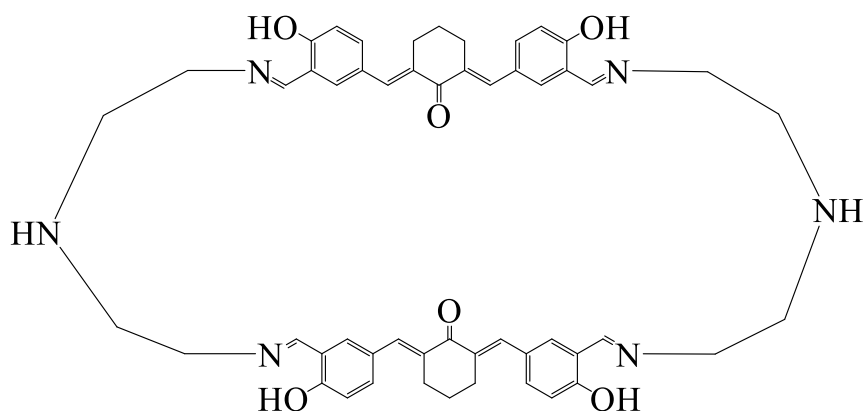


Figure. 4.6. Structure of Tetraaminocorand.

By using FT-IR, <sup>1</sup>H NMR, <sup>13</sup>C NMR, DEPT135, HRMS, and SC-XRD techniques, the structure of the resultant corand was characterized.

FT-IR spectrum of tetraaminocorand shows phenolic -OH stretching around 3418.93. The IR band of phenolic -OH in parent bis-aldehyde was observed at 3214.61 cm<sup>-1</sup> (chapter 2, spectrum 2.3) which is shifted to higher wavenumber at 3418.93 cm<sup>-1</sup> (spectrum 4.1) due to extensive intramolecular hydrogen bonding between phenolic -OH and imine nitrogen. A stretching band of imine functionality appears at 1635.38 cm<sup>-1</sup>. The asymmetric and symmetric stretching of -CH<sub>2</sub> is observed at 2923.28 cm<sup>-1</sup> and 2862.19 cm<sup>-1</sup> respectively. The asymmetrical alkene group shows stretching at 1594.41 cm<sup>-1</sup> due to the extended conjugation.

The <sup>1</sup>H NMR spectra showed 10 peaks which suggest a symmetrical nature of tetraaminocorand (spectrum 4.2). The peak of aldehydic proton observed in <sup>1</sup>H NMR spectrum of bis-aldehyde at 9.96 ppm (chapter 2, spectrum 2.4) is disappeared in the <sup>1</sup>H NMR spectrum of tetraaminocorand and a new peak of imine proton is observed at 8.19 ppm (spectrum 4.2).

---

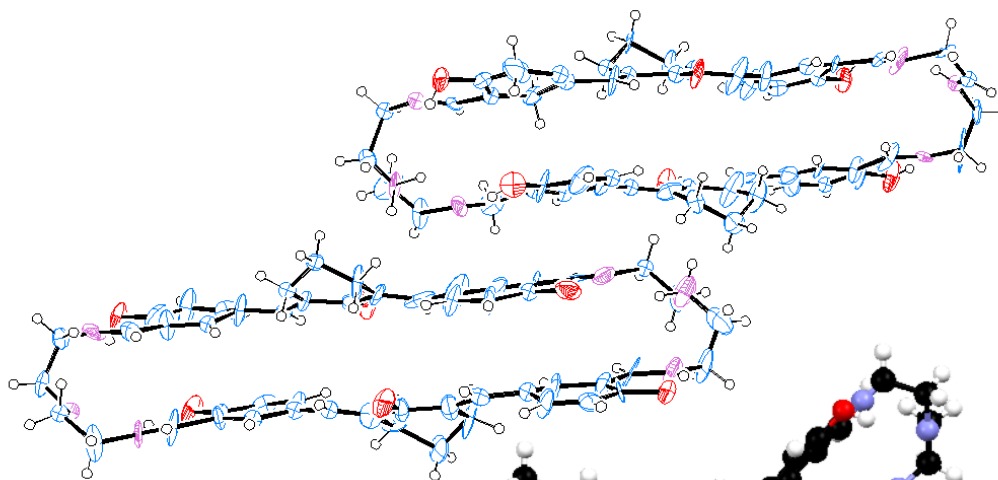
The proton of the phenolic hydroxyl group in the  $^1\text{H}$ NMR spectrum of bis-aldehyde appeared at 11.91 ppm (chapter 2, spectrum 2.4) is moved downfield to 13.58 ppm in  $^1\text{H}$ NMR spectrum of tetraaminocorand due to intramolecular hydrogen bonding interaction with imine moiety. In an aromatic region a singlet of a vinylic proton attached to the carbon containing aromatic ring is observed at 7.60 ppm. A double doublet is observed at 7.42 ppm with coupling constant 8.4 Hz and 2.0 Hz corresponds to an aromatic proton para to imino group indicating ortho and meta coupling respectively. A doublet at 6.93 ppm with coupling constant 1.6 Hz corresponds to aromatic proton ortho to imino group and a doublet at 6.79 ppm with coupling constant 8.8 Hz corresponds to aromatic proton meta to imino group. A singlet at 3.73 ppm corresponds to methylene proton attached to imine moiety while a triplet at 3.00 ppm corresponds to the methylene proton attached to secondary nitrogen. The methylene protons of cyclohexanone moiety appear as a triplet at 2.72 ppm and as a multiplet around 1.73-1.63 ppm. We should have got a quintet for methylene proton around 1.6 ppm but it results in a multiplet due to getting merged with water present in  $\text{CDCl}_3$ .

The symmetrical structure of tetraaminocorand is likewise represented by the 14-peak in  $^{13}\text{C}$  NMR (spectrum 4.3) and 9 peaks in DEPT135 spectrum (spectrum 4.4).

The [2+2] cyclocondensation was also confirmed by the HRMS  $[(M/2)+1]$  peak at 430.2131 (spectrum 4.5). The tetraaminocorand has two secondary nitrogen which can be protonated to get +2 charge hence m/z value is half than the exact mass of the tetraaminocorand.

From SC-XRD investigation, the structure of tetraaminocorand was determined. Dichloromethane was slowly evaporated in order to crystallise the tetraaminocorand. The structure analysis showed that two moiety of bis-aldehyde joined with two moiety of  $\text{N}^1$ - (2-aminoethyl)ethane-1, 2-diamine via an imine linkage and thus produced an rectangular curved shape cavity with the dimension of 6.541 Å x 19.593 Å (figure 4.7).

A.



B.

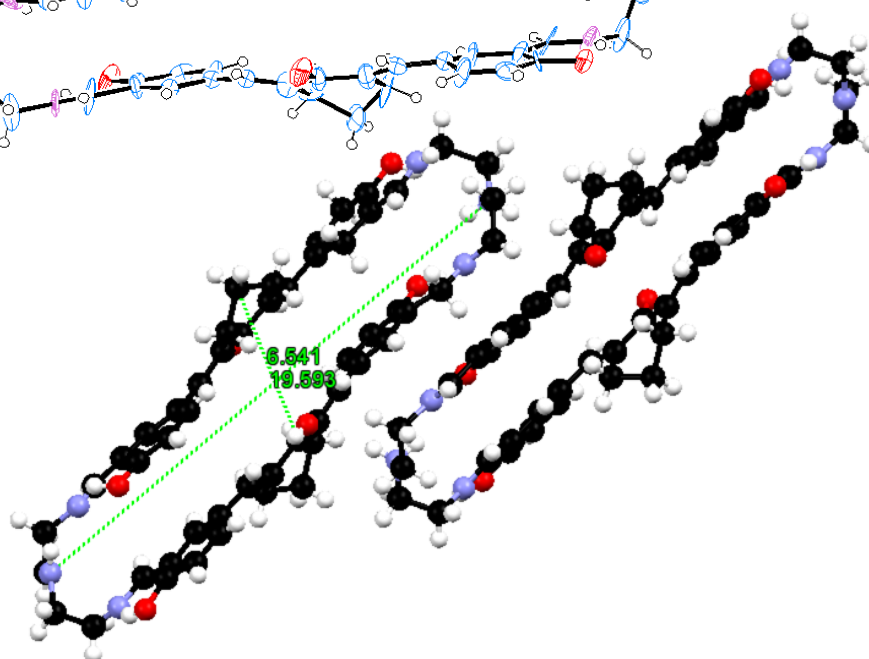


Figure. 4.7. A.) ORTEP diagram of Tetraaminocorand, B.) Intrinsic cavity dimension of Tetraaminocorand.

The C=N bond has a bond length of roughly 1.27 Å, which is the average bond length for imine bonds. The tetraaminocorand crystallises in triclinic crystal system with  $P-1$  space group and the asymmetric unit contains two unit of macrocycle (table 4.A.1). In third chapter, we have synthesized a macrocycle from TREN(Tris-2-aminoethylamine) and bis-aldehyde (chapter 3, figure 3.4) which crystallised in monoclinic crystal system with  $P2_1/c$  space group and the asymmetric unit contained one unit of macrocycle.

Empirical formula	C <sub>52</sub> H <sub>54</sub> N <sub>6</sub> O <sub>6</sub>
Temperature (K)	293
Crystal system	triclinic
Space group	<i>P</i> -1
a (Å)	6.988(7)
b (Å)	14.837(10)
c (Å)	20.740(14)
α (°)	87.82(4)
β (°)	89.79(5)
γ (°)	90.00(7)
Volume (Å <sup>3</sup> )	2148.77
Z	4

Table. 4.A.1. Crystal data of tetraiminocorand.

The lack of one arm of diethylenetriamine group in tetraiminocorand increases the size of intrinsic cavity. In the crystal structure of intermediate bis-aldehyde, both aromatic ring are not in the same plane, similar pattern is also observed in the crystal structure of hexaminocryptand (chapter 3, figure 3.4) in which aromatic rings of one of the three arms are not in the same plane but in the crystal structure of tetraiminocorand the two aromatic rings of any single arm are in the same plane. The cyclohexanone showed a half chair form. The disorientation pattern of cyclohexanone ring in the crystal structure of tetraiminocorand and hexaminocryptand are similar. The diethylene moiety of tetraiminocorand induces more flexibility as compared to tetraiminochiralcorand (chapter 2, figure 2.13) where the presence of DACH moiety doesn't provide enough flexibility. This additional flexibility might help to accommodate the guest molecule. The dimension of cavity of tetraimniocorand is also larger than the tetraiminochiralcorand which provides more space for the encapsulation of bulkier guest molecule. The aromatic rings of two arms of tetraiminocorand doesn't overlap over each other as in case of tetraiminochiralcorand and hexaminocryptand. The carbonyl group of cyclohexanone rings of both arms point in one direction, while hydroxyl group of aromatic rings are arranged in 1, 2-alternate manner. It is observed that the tetraiminocorand resembles 1, 2-alternate conformer of calixarene while tetraiminochiralcorand resembles 1, 3-alternate conformer of calixarene. In order to develop an MRI-guided drug delivery system we loaded MRI T1 contrast agent, gadolinium ion with anticancer drug flufenamic acid by kneading approach. For better understanding of binding of gadolinium ion with the corand, we performed

---

UV-Vis titration. Tetraaminocorand molecule showed the absorbance maximum at 365.94 nm (figure 4.8).

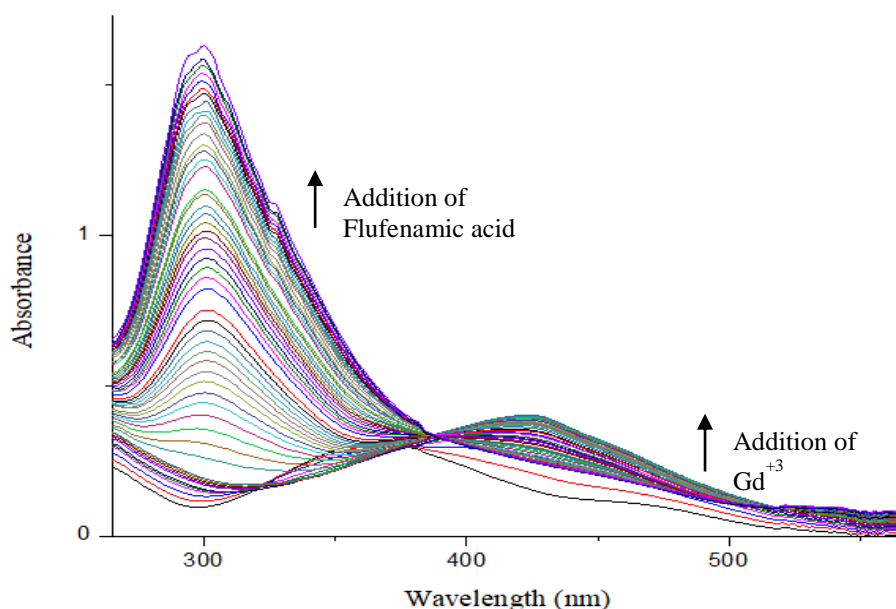


Figure. 4.8. UV-Vis titration of Tetraaminocorand with Gd<sup>3+</sup> and Flufenamic acid.

On binding with gadolinium, the absorbance peak of tetraaminocorand molecules shows bathochromic and a hyperchromic shift. A bathochromic shift was observed from 365.94 nm to 422.58 nm. The addition of gadolinium gives one isobestic point at 321.26 nm. When flufenamic acid was added into the same solution, the absorbance peak of gadolinium loaded tetraaminocorand showed hypsochromic and hypochromic shifting with the generation of a new peak. The hypsochromic shift from 422.58 nm to 298.63 nm was observed. The addition of flufenamic acid gives one isobestic point at 387.49 nm. The encapsulation of gadolinium is also confirmed by the FT-IR spectroscopy (spectrum 4.6). After encapsulation of gadolinium ion, the stretching frequency of imine bond of tetraaminocorand shifted from 1635.38 cm<sup>-1</sup> (spectrum 4.1) to 1652.34 cm<sup>-1</sup> (spectrum 4.6). The shifting of imine band suggests the coordination of gadolinium ion with salen residue of the tetraaminocorand. After encapsulation of flufenamic acid, imine stretching frequency of Gd-corate shifted from 1652.34 cm<sup>-1</sup> (spectrum 4.6) to 1639.71 cm<sup>-1</sup> (spectrum 4.7). The shift in the IR band of imine moiety of Gd-corate reveals the interaction between flufenamic acid and Gd(III) ion which affects its coordination interaction with imine moiety (spectrum 4.7 and spectrum 4.8). Isotopic ESR

---

spectrum of Gd-corate (spectrum 4.9) with  $g_{av}$  2.20 for Gd (III) was obtained. As Gd has many isotope with almost equal abundance, no effective hyperfine coupling could be seen. The drug loading capacity of the Gd-corate molecule was found to be 62 % for the drug flufenamic acid. The encapsulation efficiency of flufenamic acid was found to be 91 %.

To simulate the sustained release of flufenamic acid from Gd-corate at two different pH environments, pH 7.4 which mimics the human physiological medium and pH 5.5 which mimics the microenvironment of cancer cell, cumulative release of drug were done in phosphate buffer media in a 0.1 to 0.5 kD dialysis bag and were monitored by UV-Vis spectrophotometer. The amount of flufenamic acid released was determined using the calibration plot of the pure flufenamic acid in PBS.

In 7.5 hours, 20.82 % of flufenamic acid was released at pH 7.4, but 57.63 % of flufenamic acid was released at pH 5.5 (figure 4.9). After 8 hours, Gd-corate demonstrated the sustained release of flufenamic acid at both pH levels. At pH 7.4, total 31.22 % flufenamic acid was released whereas at pH 5.5, cumulative release of 66.32 % was observed in 24 hours. A sustained release of flufenamic acid is obtained due to its strong interaction with Gd-corate. The preferential more release of drug at pH 5.5 than the release at pH 7.3 is advantageous and can be correlated to preferential release of drug at tumour sight as cancerous cell has acidic environment. The higher release of flufenamic acid at pH 5.5 must be due to protonation/hydrolysis of imine bond resulting in destruction of Gd-corate.

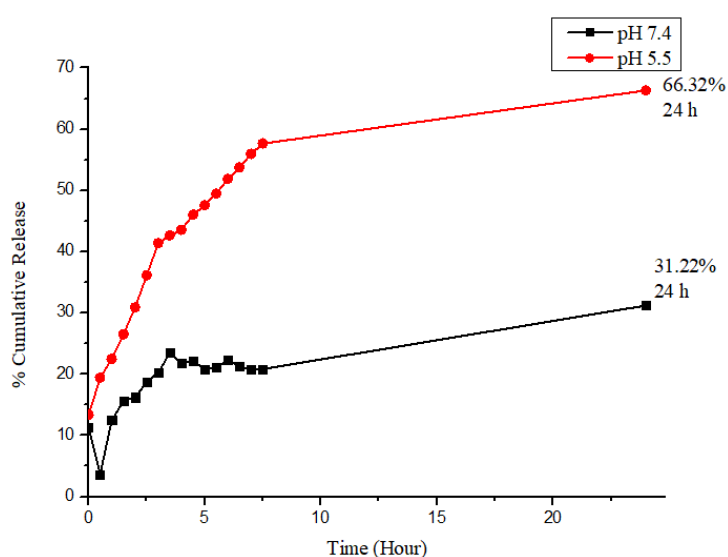
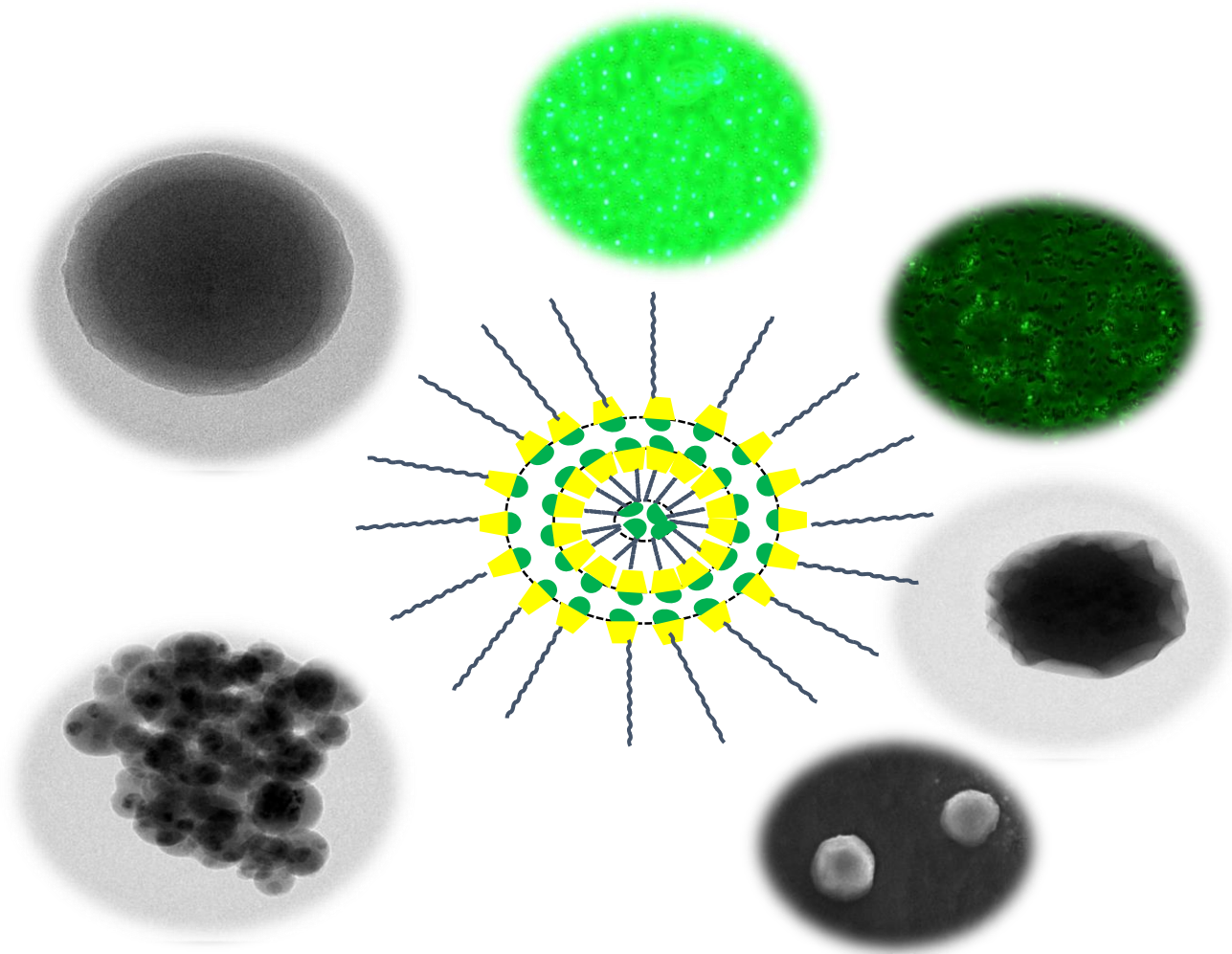


Figure. 4.9. Cumulative release profile of Flufenamic acid from Gd-corate at pH 7.4 and pH 5.5.

---

## Part B

### Synthesis of Supramolecular Vesicle



---

#### 4.B.1. Introduction

Vesicles are found everywhere in living systems and are extremely helpful in a wide range of disciplines, including chemistry, biology, and material science<sup>21-23</sup>. One of the most pressing issues in the current state of supramolecular chemistry is how to bridge the gaps between the general principles of molecular recognition/self-assembly and its use in biology and biomedical materials. Constructing vesicles with desired shapes, sizes, and properties grant them special capabilities for the creation of biomimetics, drug/genetic delivery system, and micro-reactors<sup>24-29</sup>. Recently, research on stimuli responsive supramolecular vesicles has become a particularly interesting subject, as they possess unique structures that can effectively enclose drugs, protect them from degradation, decrease their toxicity, and be released with a particular external stimulus<sup>30-40</sup>.

It is important to highlight that not all amphiphilic compounds can form vesicles due to structural factors, where the assembling morphology might be predicted by the crucial packing parameters<sup>41-46</sup>. In this regard, the supramolecular technique, "supra-amphiphiles" coined by Prof. Zhang, opens a clever, alternative way to customize the assembling morphology by the reversible non-covalent interactions, avoiding time-consuming covalent synthesis<sup>47-49</sup>. More crucially, with the clever design of the building blocks, desired buildings may be elegantly constructed and simply controlled<sup>50</sup>.

The non-covalent interactions which forms vesicles can be hydrophobic contact, hydrogen bonds, electrostatic attraction, or metal coordination. The hydrophobic interaction between the long alkyl chains in typical amphiphiles acts as the primary catalyst for the formation of these high-order aggregates. The related vesicles were therefore predominantly discovered in aqueous solution. Studies on aggregate morphology in non-aqueous liquids actually have the potential to expand the role of vesicles as a microreactor, drug delivery vehicle, and synthetic template for materials. It has been documented that vesicles can form in aprotic organic solvents, including reversed bilayer vesicles made from peptide-lipids and fluorocarbon bilayer vesicles made from fluorocarbon amphiphiles. There is, however, a paucity of studies on vesicles in protic organic media<sup>51</sup>.

Macrocyclic compounds, including crown ethers, cyclodextrins (CDs), calixarenes, cucurbiturils, pillararenes, and their analogues, can all serve as supramolecular hosts to encapsulate guest molecules into their cavities. Such host can be transformed into vesicles by

---

attachment of suitable long chain molecules and have been extensively designed and synthesized in recent years<sup>52-68</sup>.

In order to create a stable controlled release system, Rita et. al. reported a novel crown ether amphiphile. Niosomes were created using crown ether amphiphile and cholesterol. By adding the anti-cancer drug 5-fluorouracil, the applicability of these niosomes as drug delivery vehicles has been assessed. According to *in vitro* research, encapsulating a medicine in niosomes resulted in a sustained drug release as compared to a free solution<sup>69</sup>.

In order to deliver phenytoin sodium to the eyes with minimum drug-induced irritability and increased efficacy, Dina et. al. created innovative crown ether-based nanovesicles called "Crownsomes." As a result of its small particle size and homogeneous distribution, which create a large surface area for drug solubilization, this formulation is a novel drug delivery system with high encapsulation efficiency. They also showed sustained drug release patterns and improved drug solubilization<sup>70</sup>.

By combining  $\beta$ -CD with an artificial anionic amphiphile 4-(4-(hexyloxy)phenylazo)benzoate sodium (HPB) with an azobenzene and carboxylate groups, Wang et. al. created quintuple-responsive vesicles. The photo/pH responsiveness of HPB, competitive host-guest complexing, amylase-catalyzed  $\beta$ -CD hydrolysis, and host-guest interaction between the alkyl chain of HPB@  $\beta$ -CD and  $\beta$ -CD allowed for the production of vesicles that were responsive to UV light, pH,  $\beta$ -CD, amylase, and 1-adamantane carboxylic acid sodium (ADA)<sup>71</sup>.

p-sulfonatocalix[8]arene and chitosan-based supramolecular amphiphilic vesicles were created by Ahire et. al. through electrostatic contact between the anionic calixarene and cationic chitosan molecules<sup>72</sup>.

Mannosylated amphiphilic pillar[5]arene (Man@AP5), synthesized by Peng et. al., self-assembles into supramolecular vesicles. Vancomycin (Van), which targets macrophages, was enclosed in a vesicle (Man@AP5-Van). The vesicle responds to acid and cathepsin B to release vancomycin inside macrophages. Man@AP5-Van greatly boosts the intracellular concentration of Van, in results increasing its antibacterial activity against intracellular MRSA (Methicillin-resistant *S. aureus*)<sup>73</sup>.

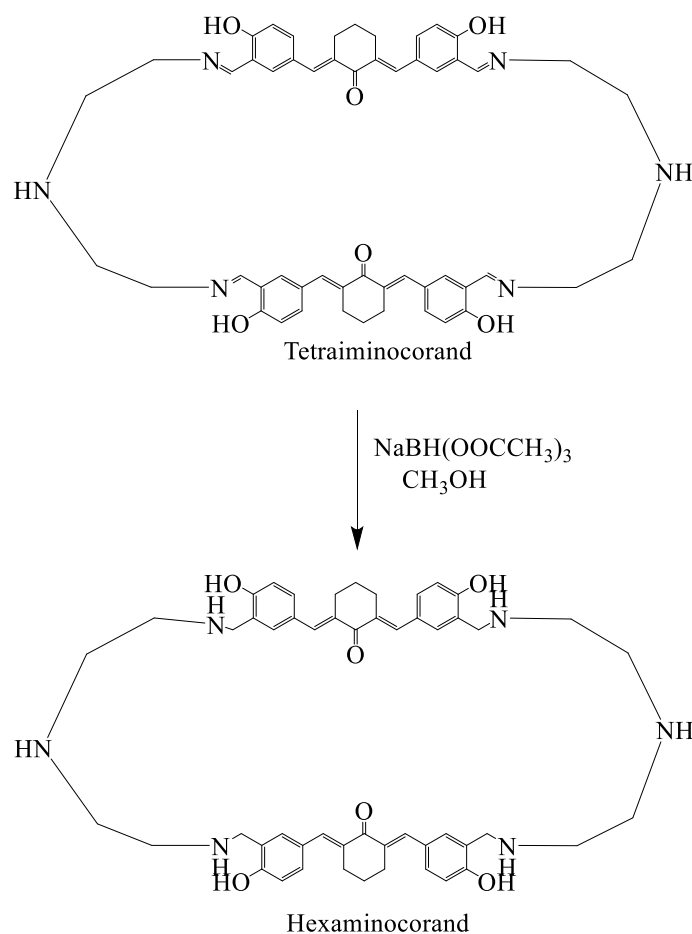
---

## 4.B.2. Experimental Section

### 4.B.2.1. Materials

The chemicals and solvents used in the preparation of curcuminoid based vesicle were of analytical grade and purchased from Merck, Spectrochem, Loba chemicals, TCI and SRL. Chemicals were used without further purification.

### 4.B.2.2. Reduction of Tetraiminocorand



Scheme. 4.2. Reduction of Tetraiminocorand.

The tetraiminocorand (1 g, 0.0011 moles) was dissolved in 100 ml DCM (Dichloromethane) and 300 ml methanol. Added sodium triacetoxyborohydride (5.92 g, 0.028 moles) to magnetically stirred solution of tetraiminocorand. The solution was stirred for 5-6 hours. Methanol was evaporated under vacuum completely. Residue was quenched in liquor ammonia and extracted with DCM. The DCM layer was dried over sodium sulphate and evaporated to

---

obtain the desired product. The formed hexaminocorand was dried under high vacuum to obtain red free flowing solid.

**Yield:** 98 %

**M. P.:** 247 °C (Degraded)

**FT-IR** (KBr disc,  $\text{cm}^{-1}$ ): 3028.24( $\nu$  -OH), 2826.45( $\nu$ -CH<sub>s</sub>), 1649.53( $\nu$ -C=O), 1584.30 ( $\nu$ -C=C).

**<sup>1</sup>H NMR:** (400 MHz, DMSO-d<sub>6</sub>):  $\delta$  7.52 (1H, s), 7.31 (1H, s), 7.24 (1H,  $J$  = 8.4 Hz, d), 6.74 (1H,  $J$  = 8.0 Hz, d), 4.80 (6H, bs), 3.82 (2H, s), 2.76- 2.66 (6H, m), 1.60 (1H, s).

**<sup>13</sup>C NMR:** (400 MHz, DMSO-d<sub>6</sub>):  $\delta$  188.45, 174.29, 136.64, 133.08, 131.98, 131.50, 125.88, 125.09, 116.29, 49.64, 47.96, 47.74, 28.45, 23.07.

#### **4.B.2.3. Pegylation of Hexaminocorand**

10 mg (0.0115 mmol) of hexaminocorand was dissolved in 5 ml mixture of butanol:water(1:4). 14.53  $\mu$ l (0.0242 mmol) of PEG-600 diacarboxylic acid was added into the solution of hexaminocorand and sonicated for 5 minutes at room temperature. The colour of dispersion instantly changed from red to pale yellow confirming the formation of pegylated hexaminocorand. The resultant solution was dried under vacuum for 3-4 days.

#### **4.B.2.4. Formation of Vesicle and Encapsulation of Capecitabine**

10.6 mg (0.000722 mmol) of pegylated hexaminocorand was dissolved in 5 ml of conductivity water. The drug capecitabine was added into the solution of vesicle in different amount such as 0.5 mg (1:5::blank vesicle:capecitabine), 1 mg(1:10::blank vesicle:capecitabine), and 10.29 mg (1:100::blank vesicle:capecitabine), sonicated for 10 min at room temperature.

#### **4.B.2.5. Calculation of Drug Loading (DL%) of Vesicle and Encapsulation Efficiency (EE%) of Capecitabine**

2 ml of vesicle with different ratio of capecitabine in aqueous solution was dialysed using a dialysis bag (MWCO: 500 da) in 100 ml of aqueous medium at 37°C to calculate the drug loading and encapsulation efficiency. UV- Vis spectrophotometer was used to quantify the amount of drug contained in the vesicle. The concentration of free drug was determined by withdrawal of 5 ml of release medium and measuring absorption at 303 nm on UV-spectrophotometer. The calibration plot for capecitabine was used to determine the

---

concentration of drug released (Unbound drug) in aqueous medium. The concentration of unbound drug was subtracted from the drug added to the carrier to determine the amount of drug loaded. Using the following formulae<sup>74</sup>, the drug loading (DL) and entrapment efficiency (EE) were calculated in comparison to calibration plot of capecitabine:

$$DL (\%) = [(W_{\text{Capecitabine}} - W_{\text{Unbound Capecitabine}}) / W_{\text{Capecitabine loaded vesicle}}] \times 100$$

$$EE (\%) = [(W_{\text{Capecitabine}} - W_{\text{Unbound Capecitabine}}) / W_{\text{Capecitabine}}] \times 100$$

Where,

$W_{\text{Capecitabine}}$  = Weight of capecitabine in inclusion complex

$W_{\text{Unbound Capecitabine}}$  = Weight of unbound capecitabine released from vesicle

$W_{\text{Capecitabine loaded vesicle}}$  = Weight of capecitabine loaded vesicle

#### **4.B.2.6. Cumulative release of Capecitabine**

2 ml of vesicles with different ratio such as 1:5, 1:10, and 1:100 of pegylated hexaminocorand: capecitabine in aqueous solution were dialysed using a dialysis bag (MWCO: 500 da) in 100 ml of the buffer solution at 37°C. The study was carried out with PBS (Phosphate buffer solution) of pH 7.4 and PBS of pH 5.5. PBS of pH 7.4 mimics the normal physiological medium and PBS with pH 5.5 simulates the tumour microenvironment. To determine the cumulative drug release, the UV-Vis spectrometer was used to quantify the dialysate at 303 nm during the drug release. A predefined volume of the release medium (5 ml) was withdrawn at regular intervals, and an equal volume of freshly made buffer was then supplied to make up for this withdrawal.

#### **4.B.2.7. Characterization Method**

FT-IR studies of all compounds were performed on Bruker Alpha FT-IR spectrometer in solid state as KBr pellets. UV-visible Spectrophotometer experiments were performed on Perkin Elmer Lambda 35 Spectrophotometer, Inc, MA, USA. NMR data was recorded on Bruker AVANCE, 400 MHz spectrometer in CDCl<sub>3</sub> and DMSO-d<sub>6</sub>, with TMS as internal standard.

---

### 4.B.3. Result and discussion

Although several kinds of non-covalent interactions have been used to fabricate supramolecular amphiphiles and vesicles from synthetic precursors, the vesicle formation by utilising analogue of natural products, have been much less frequently explored in the field of drug delivery.

We are first to developed a vesicle from curcuminoid based macrocycle. In doing so, the tetraaminocorand was reduced to hexaminocorand and derivatised with PEG to form vesicles.

The selective reduction of imine bonds of tetraaminocorand were achieved in the presence of sodiumtriacetoxy borohydride at room temperature (scheme 4.2) (figure 4.10).

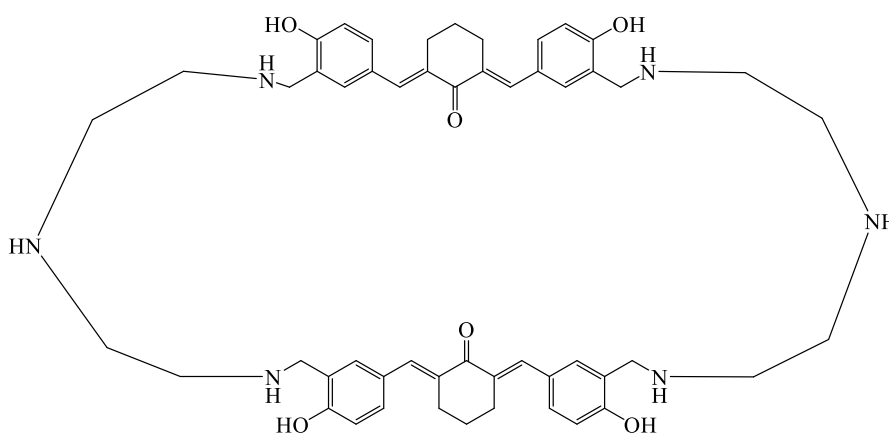


Figure. 4.10. Structure of Hexaminocorand.

The reduction of imine bond was further characterized by FT-IR and NMR techniques. The characterization from FT-IR spectrum showed the disappearance of  $-C=N$  stretching and appearance of  $-NH$  stretching at  $3028.24\text{ cm}^{-1}$  which merges with the stretching frequency of  $-OH$  group of hexaminocorand (spectrum 4.10). The reduction of imine bonds was also confirmed by NMR technique. In the  $^1\text{H}$  NMR spectrum of hexaminocorand the peak of imine proton vanishes at 8.19 ppm and the peak due to methylene protons of reduced imine appears as a singlet at 3.81 ppm (spectrum 4.11). The  $^{13}\text{C}$  NMR spectrum of hexaminocorand showed total 14-peaks which suggests a symmetrical structure (spectrum 4.12). The  $^1\text{H}$  NMR spectrum of pegylated hexaminocorand showed that the aromatic proton ortho to methyl amino group shifted from 7.309 ppm (spectrum 4.11) to 7.503 ppm (spectrum 4.13) and merged with the proton of alkene group of chalcone moiety while this alkene proton shifted from 7.521 ppm (spectrum 4.11) to 7.503 ppm (spectrum 4.13). The aromatic proton para to methyl amino group of hexaminocorand shifted from 7.239 ppm (spectrum 4.11) to 7.322 ppm (spectrum 4.13). The aromatic proton ortho to hydroxyl group of hexaminocorand shifted from 6.745 ppm (spectrum 4.11) to 6.849 ppm (spectrum 4.13). There was a marked change in an aliphatic

---

region due to pegylation of hexaminocorand. The aliphatic proton of cyclohexanone moiety of chalcone group shifted from 1.599 ppm (spectrum 4.11) to 1.605 ppm (spectrum 4.13).

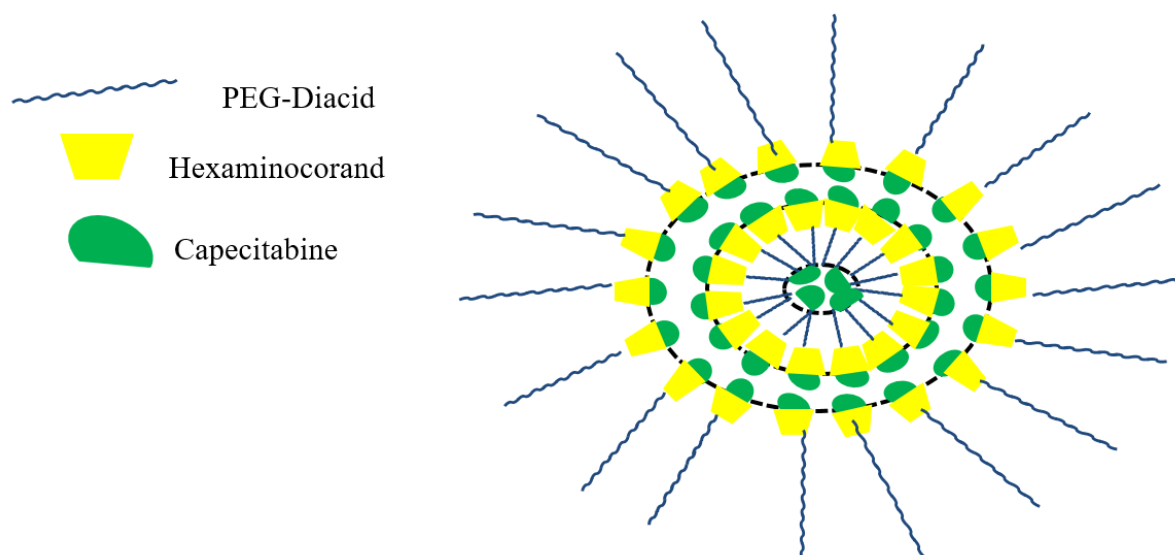


Figure. 4.11. Proposed structure of Vesicle.

The pegylated hexaminocorand self-assembled to generate vesicles in aqueous media (figure.4.11). The capecitabine was loaded on the vesicles. Capecitabine belongs to BCS class I which has high aqueous solubility and high permeability. Capecitabine has rapid and complete absorption in gastrointestinal tract but the excretion of drug and its metabolite is also rapid. The clinical viability of capecitabine is constrained despite its efficacy as an anticancer drug because of its low bioavailability, variable plasma levels, and early body elimination. Therefore, an updated sustained release delivery system is required for better plasma half-life, controlled drug release, and patient compliance in order to address the aforementioned problems with the usage of capecitabine<sup>74</sup>. In order to control release of capecitabine we loaded the vesicle with drug and characterized by FT-IR, DLS, HR-TEM, and FEG-SEM techniques. From the FT-IR spectrum it was observed that the strong stretching frequency of carbonyl group of capecitabine at  $1758.56\text{ cm}^{-1}$  (spectrum 4.15) shifted to  $1755.12\text{ cm}^{-1}$  (spectrum 4.14). The hydrodynamic diameter of 623.5 nm was observed for blank vesicle while the hydrodynamic diameter of drug loaded vesicle was found to be 518.2 nm (figure 4.12).

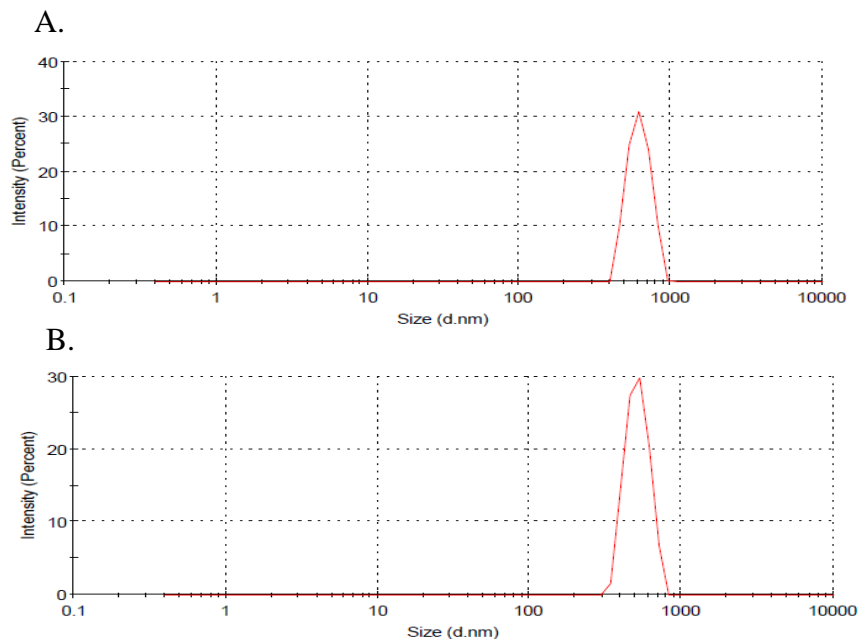


Figure. 4.12. DLS of A.) Blank vesicle, B.) Capecitabine loaded vesicle.

This reduction in diameter might be possible due to the formation of compact structure of vesicle with capecitabine which is also seen in the images obtained from HR-TEM and in FEG-SEM techniques. From the HR-TEM images the size of blank vesicle was found to be 610 nm while the HR-TEM images of drug loaded vesicle showed the size of 210 nm (figure 4.13).

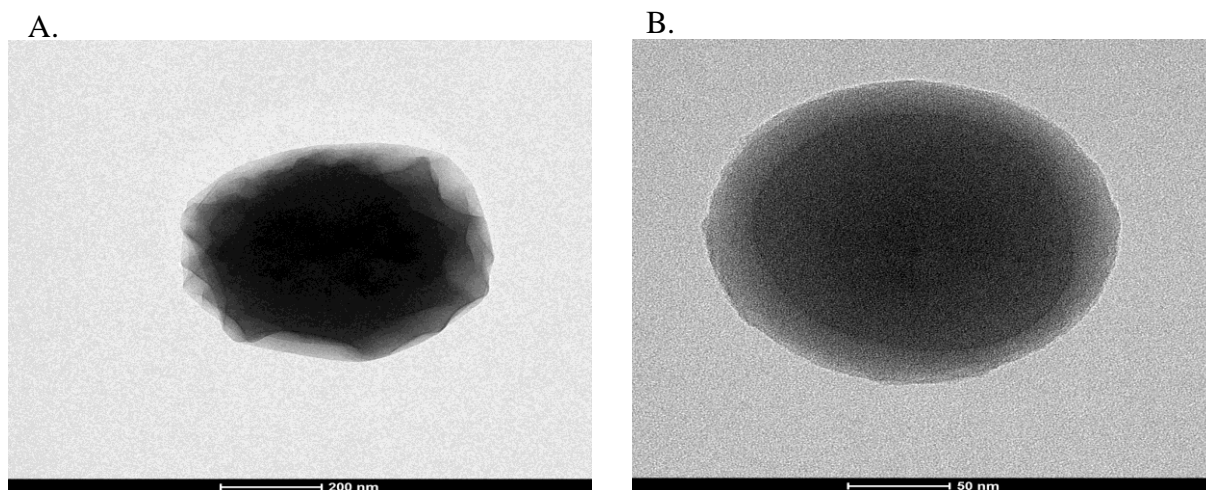


Figure. 4.13. HR-TEM images of A.) Blank Vesicle at 200 nm, B.) Capecitabine loaded vesicle at 50 nm.

The HR-TEM images revealed the star shape of blank vesicles while the drug loaded vesicles showed a spherical shape with smooth surface. Similar changes were observed in FEG-SEM images of blank and capecitabine loaded vesicles (figure 4.14).

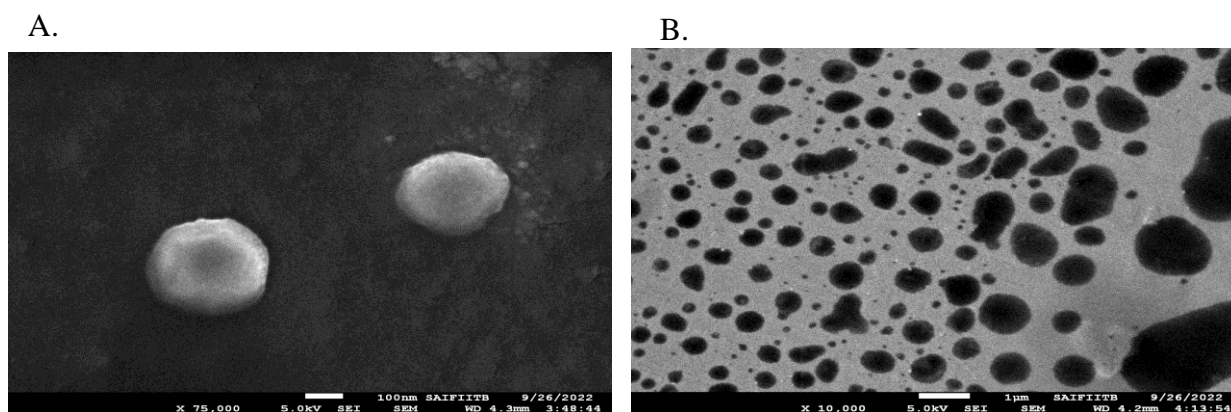
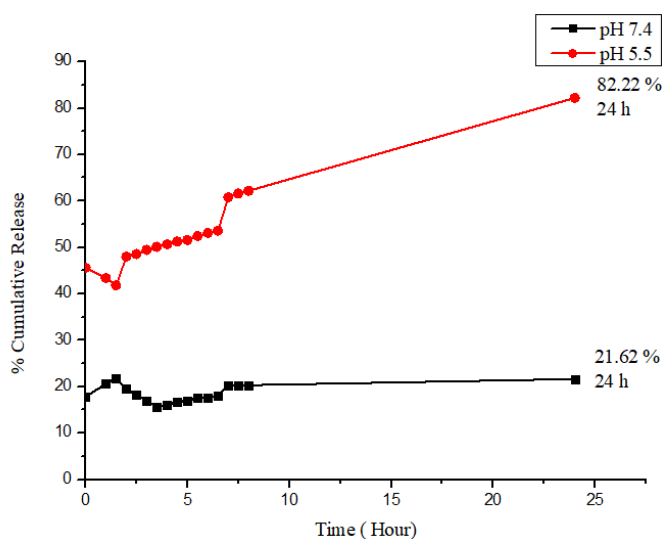


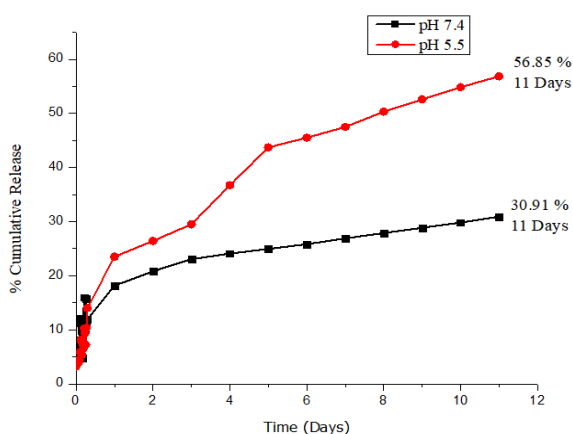
Figure. 4.14. FEG-SEM images of A.) Blank Vesicle at 100 nm, B.) Capecitabine loaded vesicle at 1  $\mu$ m.

The capecitabine was added in different stoichiometric amount to the blank vesicle to achieve 32 %, 55 %, and 82 % drug loading with 1:5, 1:10, and 1:100 blank vesicle:drug ratio respectively. To examine the release of capecitabine from vesicles with different amount of capecitabine, we performed a cumulative release experiment of capecitabine at two different pH 7.4 (human physiological medium) and pH 5.5 (tumour environment). 32 % capecitabine loaded vesicle showed the burst release at both pH 7.4 and 5.5 (figure 4.15.A) while the 55 % capecitabine loaded vesicles showed controlled release of drug over 11 days (figure 4.15.B). 30.91 % of drug was released from the vesicles at pH 7.4 while 56.85 % of the drug was released at pH 5.5. In the case of 82 % capecitabine loaded vesicles (figure 4.15.C), a significant controlled release of drug was observed. In 11 days only 2.07 % drug was released at pH 7.4 and 5.95 % drug was released at pH 5.5.

A.



B.



C.

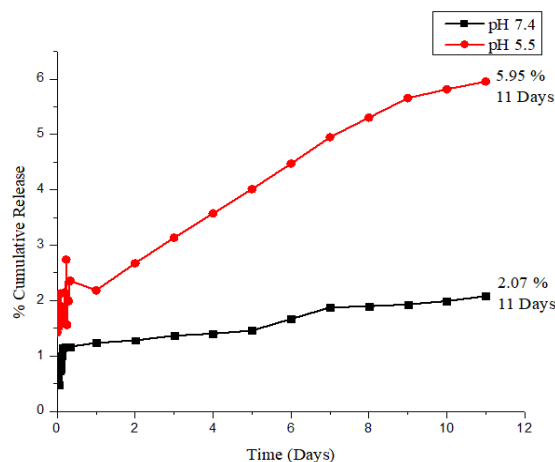


Figure. 4.15. Cumulative release profile of Capecitabine from vesicle at pH 7.4 and pH 5.5  
A.) 32 % capecitabine loaded vesicle, B.) 55 % capecitabine loaded vesicle, C.) 82%  
capecitabine loaded vesicle.

From cumulative release profile of capecitabine it is proposed that the increase in amount of drug forms more compact structure of vesicles which holds the drug molecules with strong non-covalent interactions leading to more and more sustained release of the drug. In all cases, the amount of drug released at pH 5.5 is more as compared to pH 7.4, which can be correlated to preferential release of drug at tumour site.

This behaviour supports the hypothesis that the said carrier will preferentially release capecitabine to the cancerous cells which are known to have acidic pH.

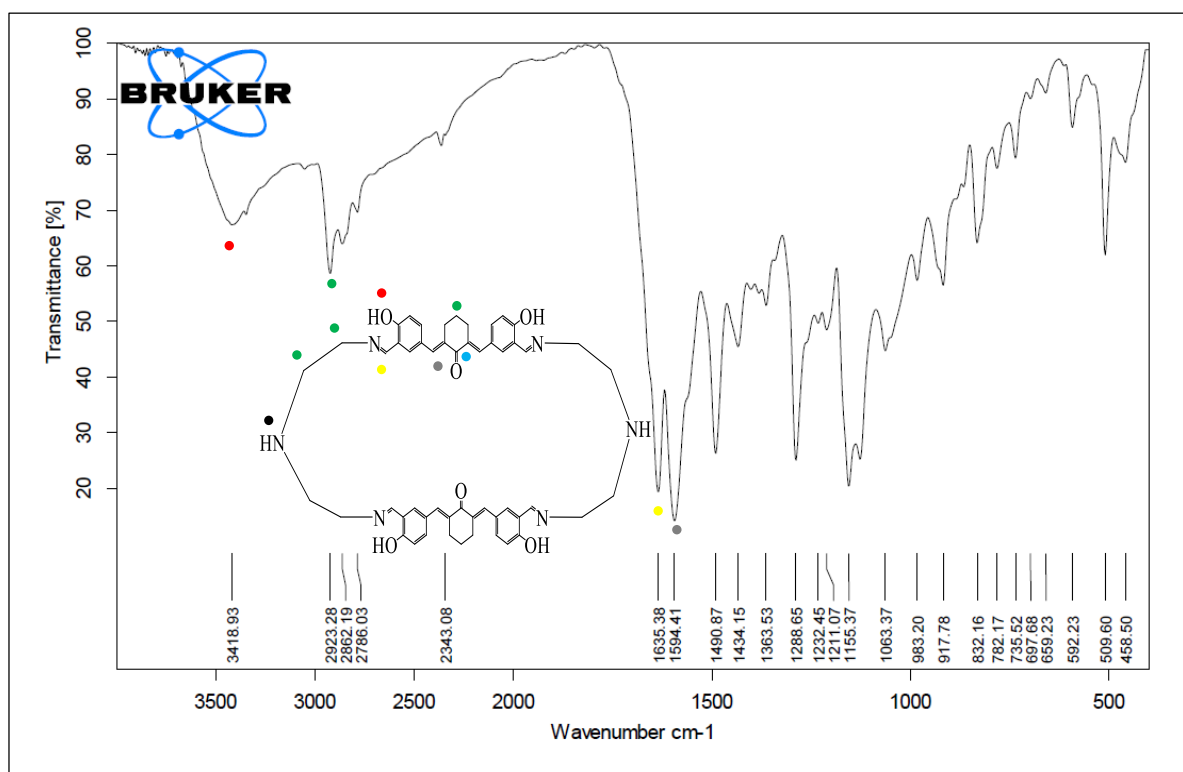
---

#### **4.4 Conclusion**

We have synthesized a curcuminoid based tetraaminocorand from high dilution method. The SC-XRD analysis showed the definite cavity dimensions of tetraaminocorand which was suitable for the loading of drug in high payload. Gadolinium and flufenamic acid were encapsulated in the cavity of the tetraaminocorand. The encapsulation of flufenamic acid in Gd-Corate was effectively monitored by UV spectroscopy. 66% drug was preferentially released at pH 5.5 in 24 hours. Further, we have selectively reduced the imine bond of tetraaminocorand. The reduced hexaminocorand got self-assembled after the pegylation and formed a vesicle in aqueous medium. The morphology of vesicle was studied by various techniques. We loaded BCS class I drug capecitabine to vesicle. The vesicle was loaded with drug capecitabine in different amount and their cumulative release was studied. The increase in drug loading results in better sustained release capacity of vesicle. The capecitabine was released preferentially higher at pH 5.5 which mimics tumor microenvironment as compare to pH 7.4 which mimics the microenvironment of normal cells.

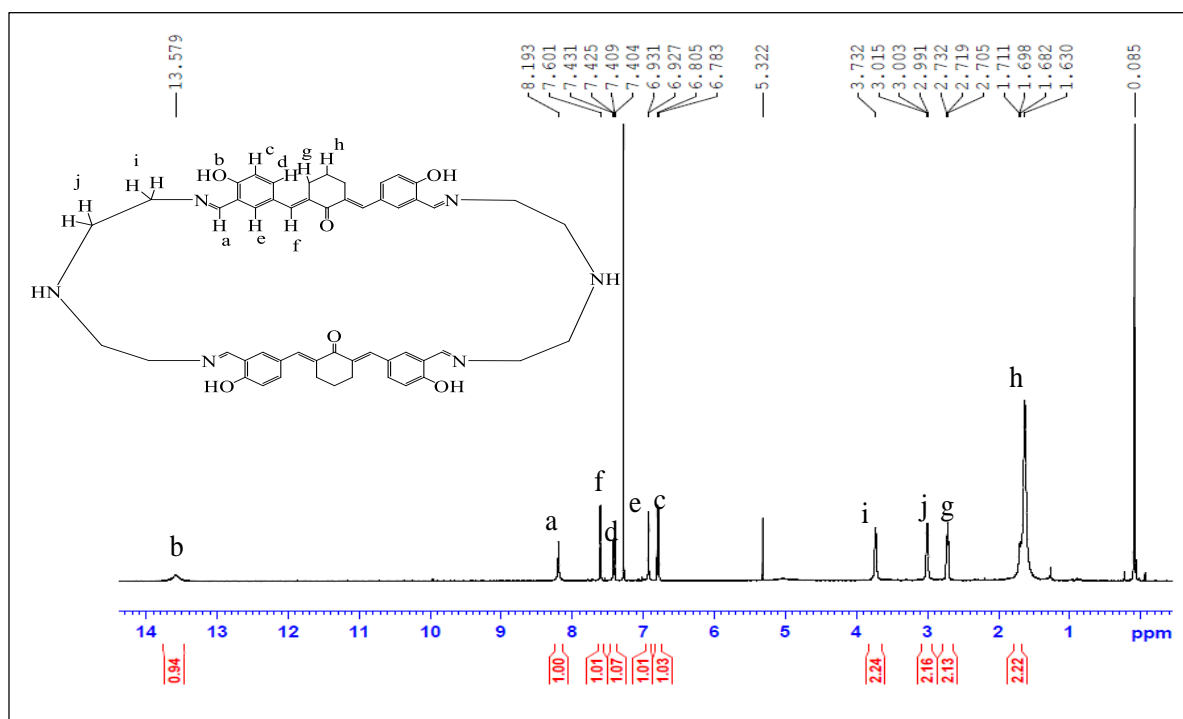
## 4.5 Analytical Data

Spectrum 4.1: FT-IR spectrum of Tetraiminocorand



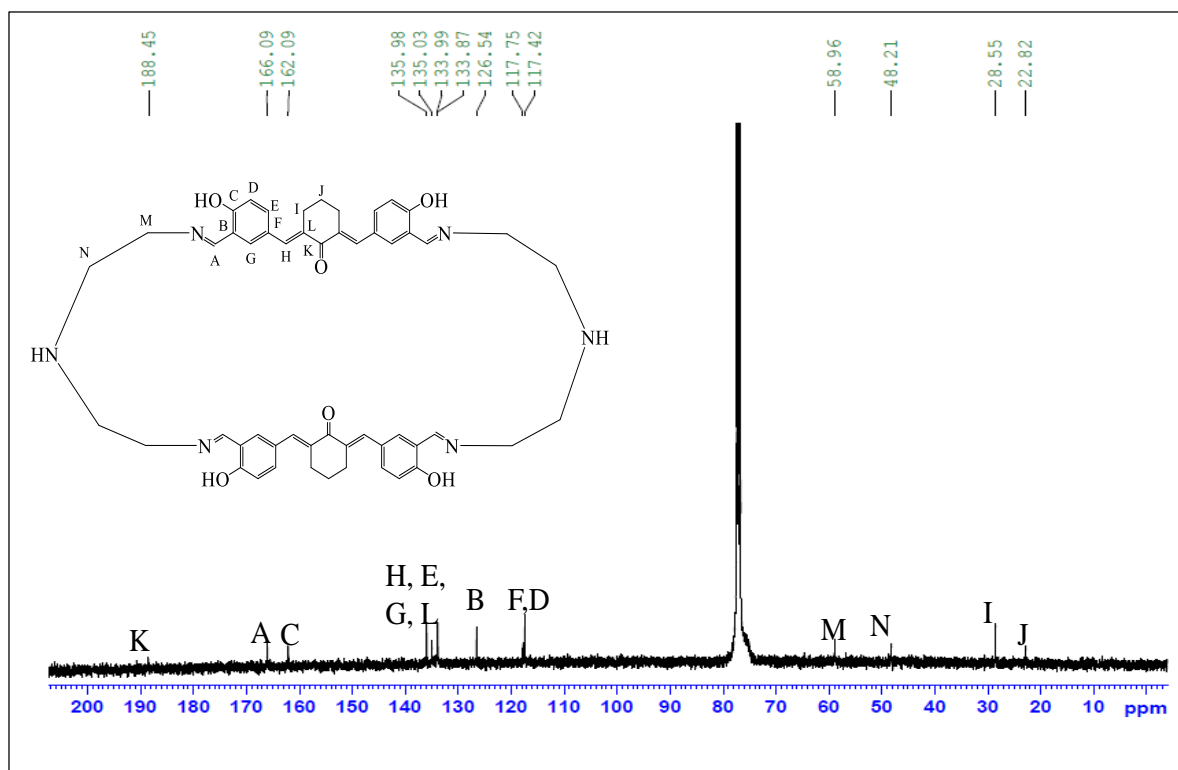
Spectrum 4.2: <sup>1</sup>H NMR spectrum of Tetraiminocorand

CDCl<sub>3</sub>



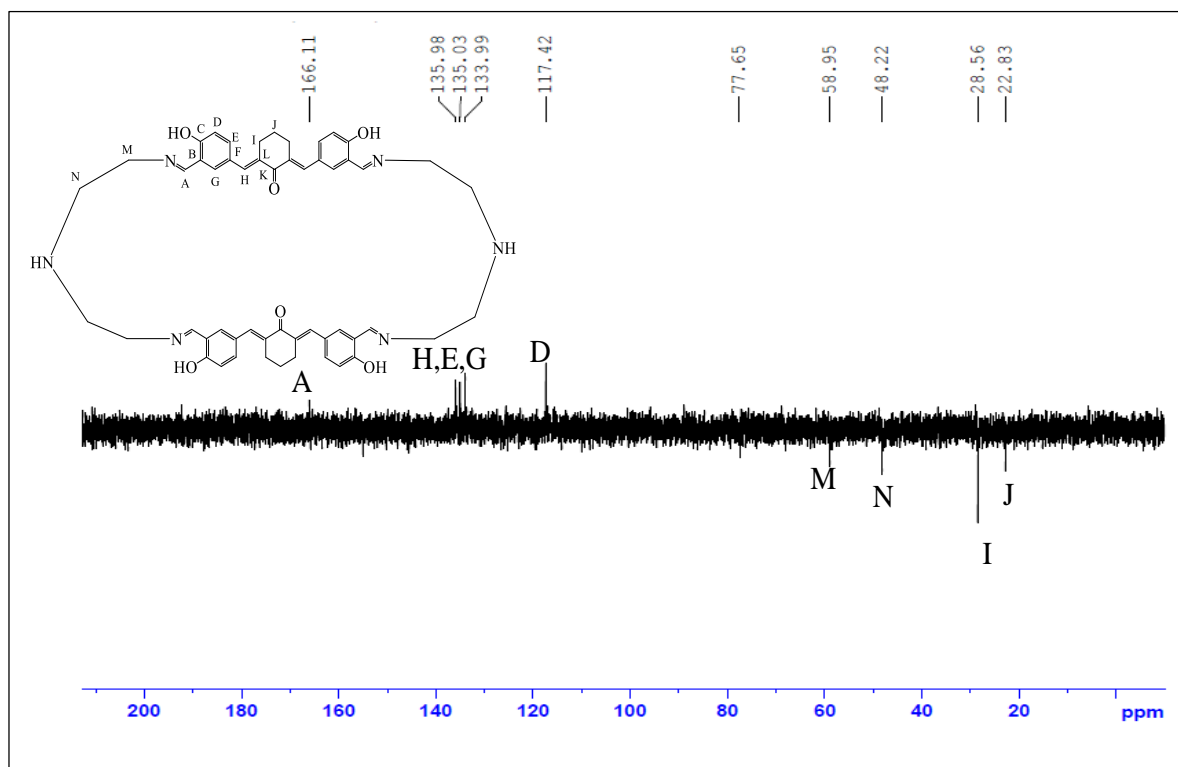
Spectrum 4.3:  $^{13}\text{C}$  NMR spectrum of Tetraaminocorand

$\text{CDCl}_3$

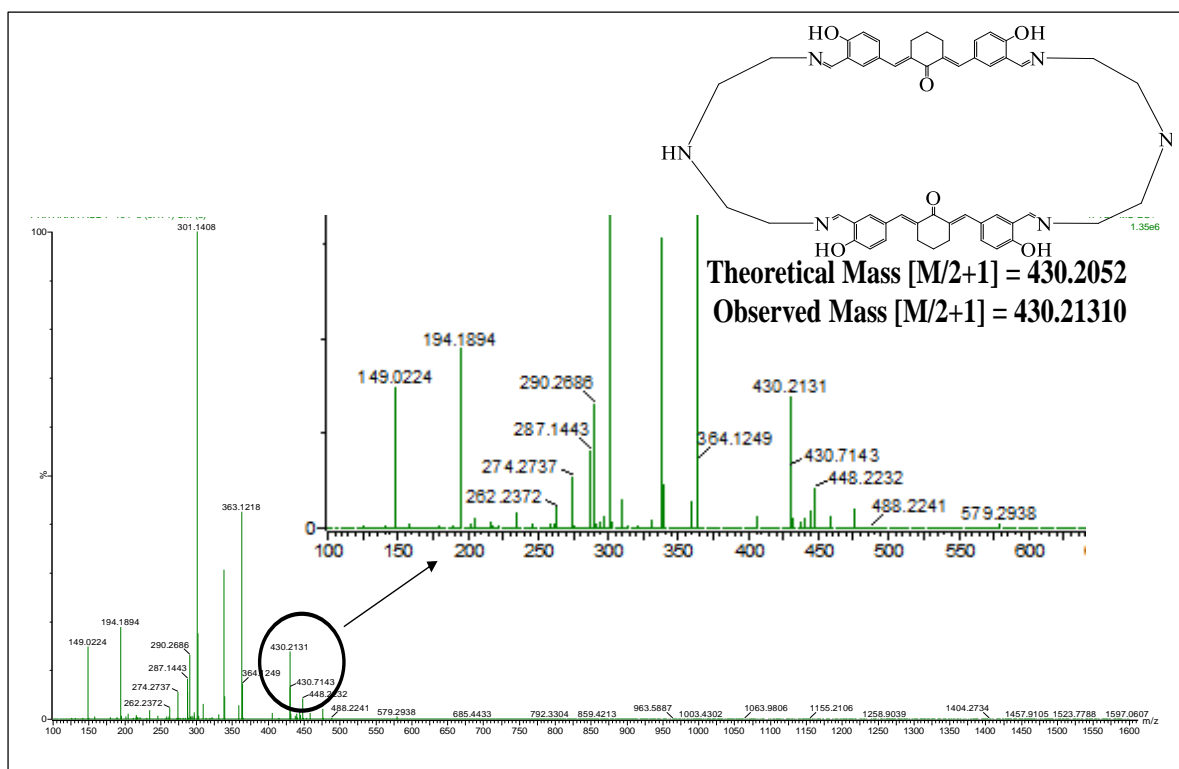


Spectrum 4.4:  $^{135}\text{DEPT}$  NMR spectrum of Tetraaminocorand

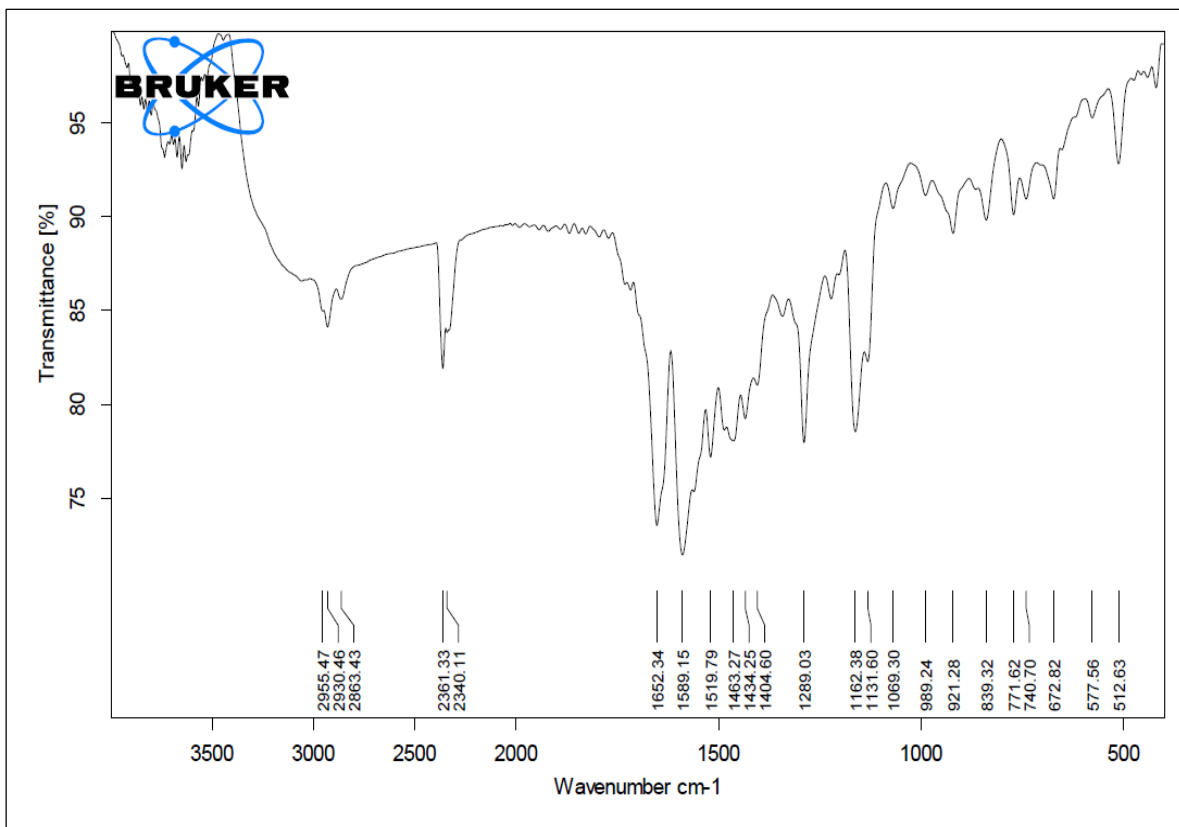
$\text{CDCl}_3$



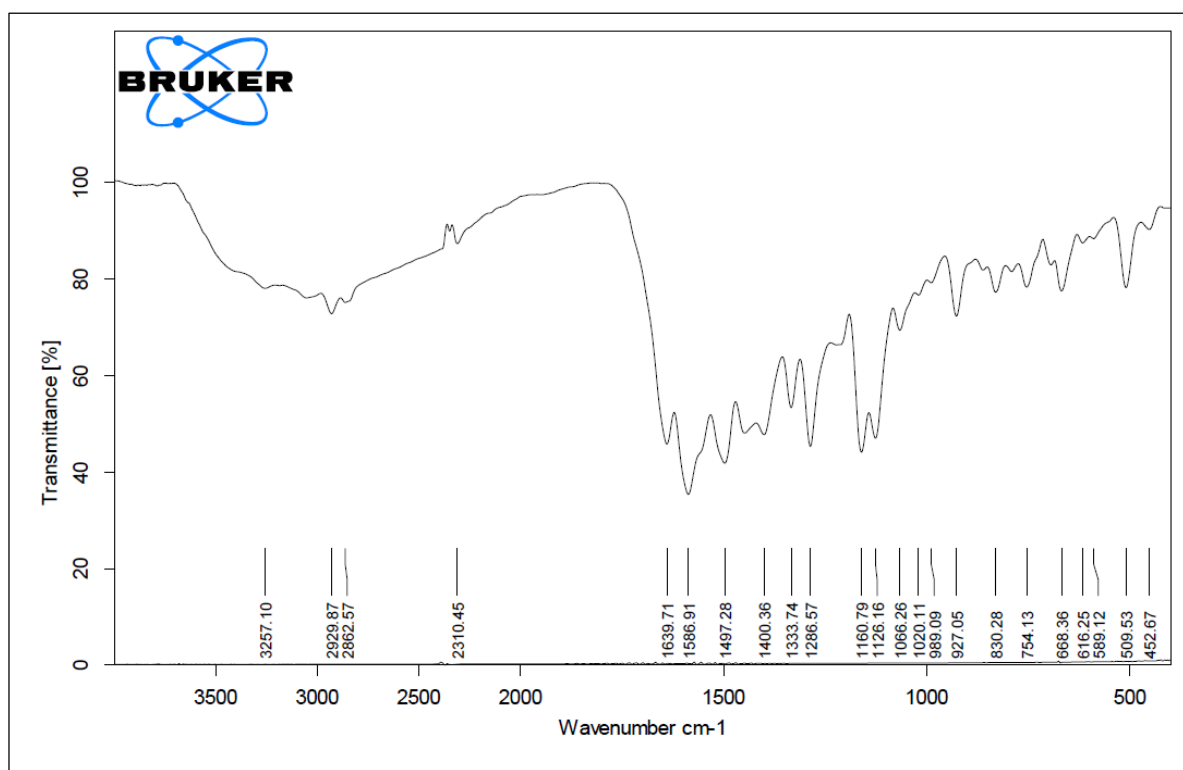
### Spectrum 4.5: HR-MS spectra of Tetraaminocorand



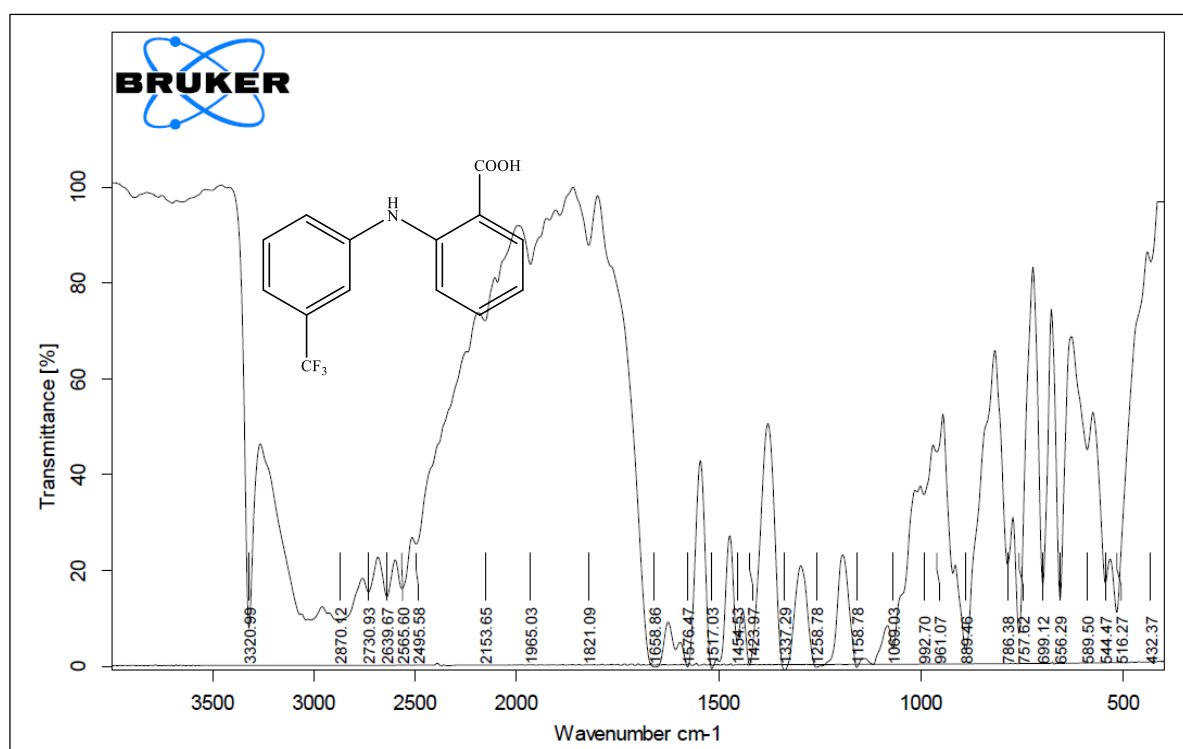
### Spectrum 4.6: FT-IR spectrum of Gd-Corate



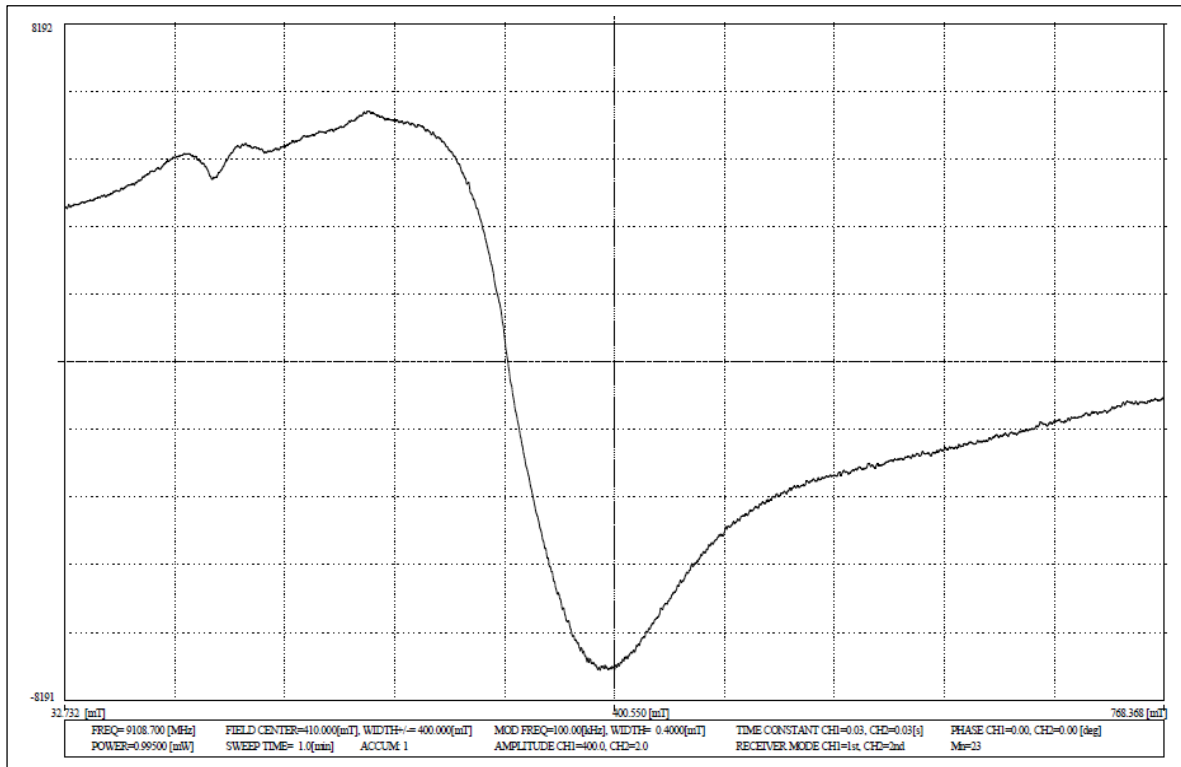
Spectrum 4.7: FT-IR spectrum of Flufenamic acid loaded Gd-Corate



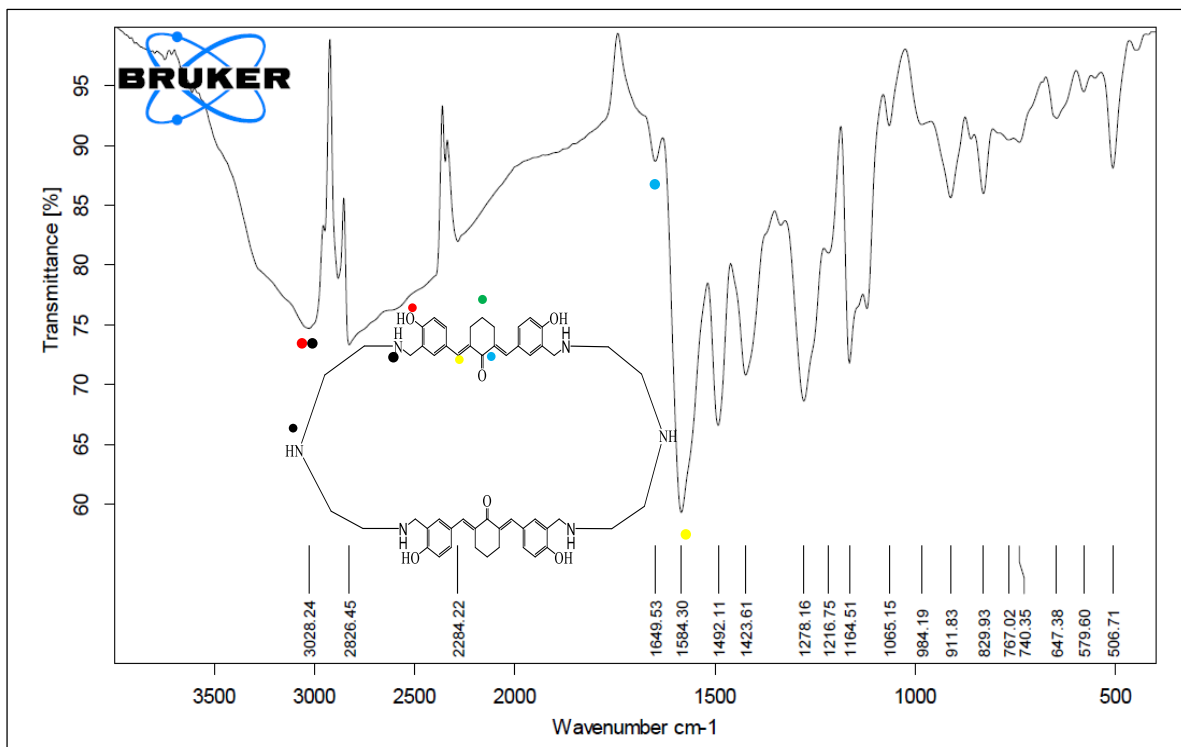
Spectrum 4.8: FT-IR spectrum of Flufenamic Acid



**Spectrum 4.9: ESR spectrum of Gd-corate**

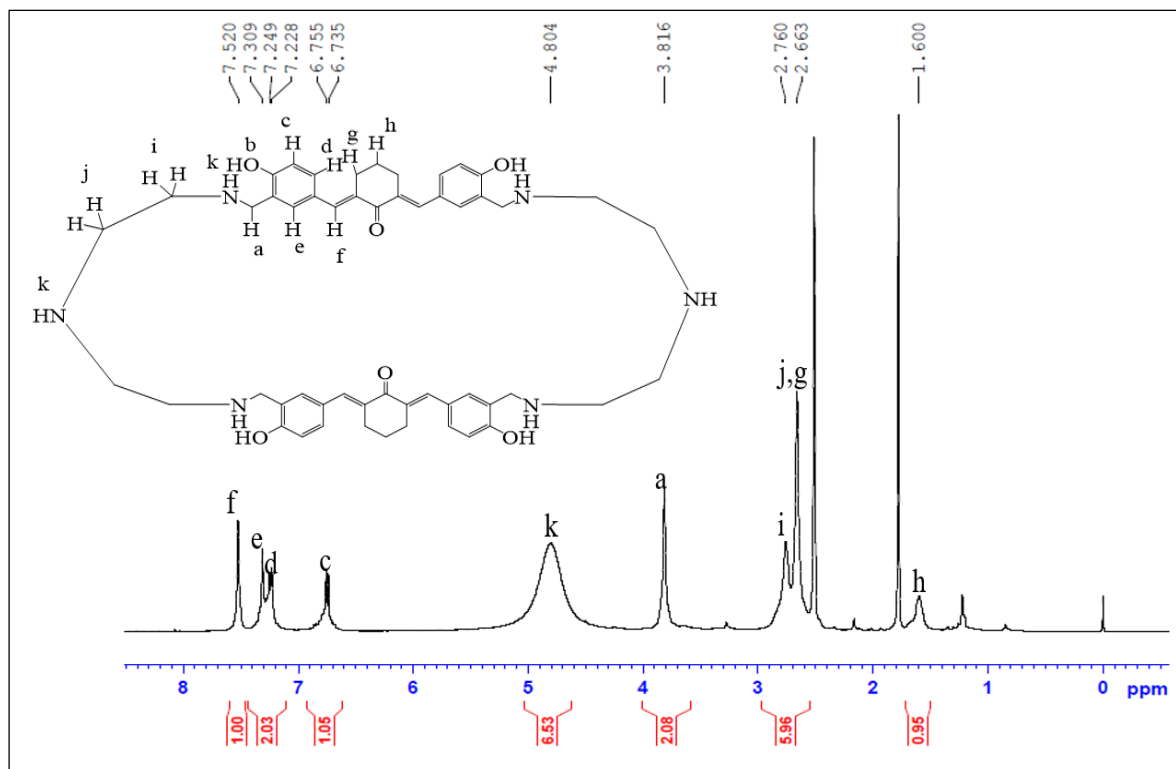


**Spectrum 4.10: FT-IR spectrum of Hexaminocorand**



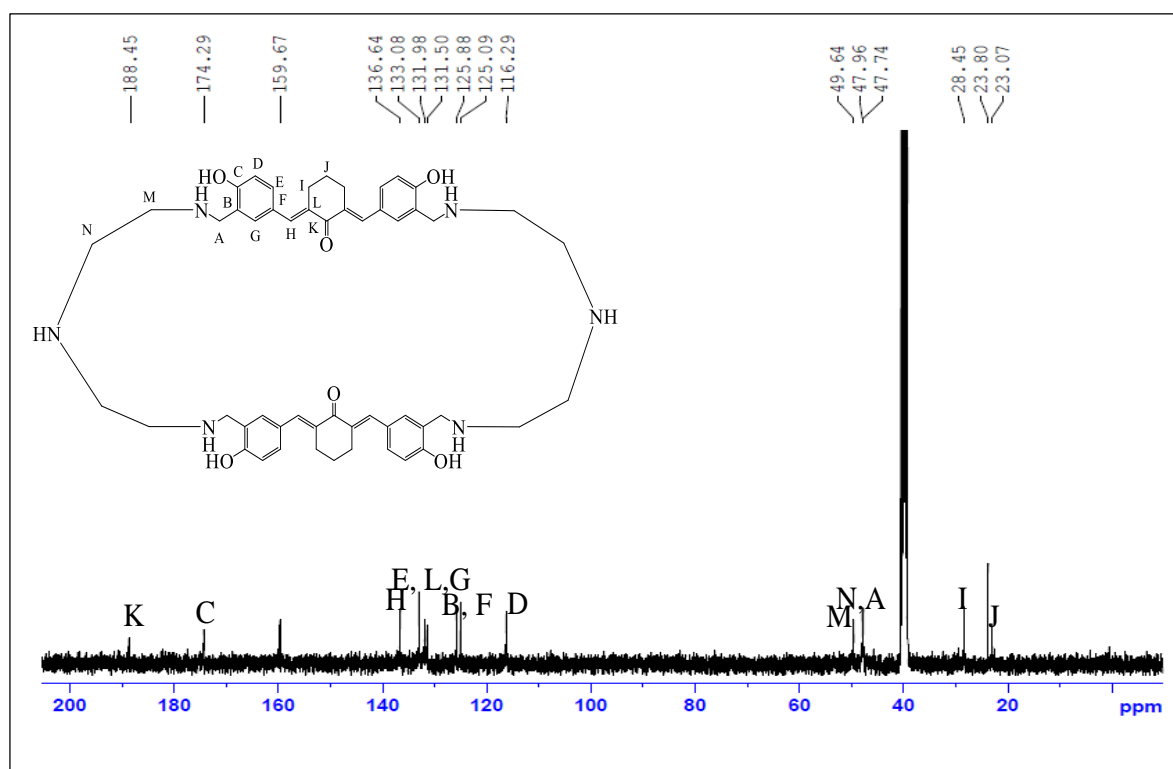
Spectrum 4.11:  $^1\text{H}$  NMR spectrum of Hexaminocorand

DMSO- $d_6$



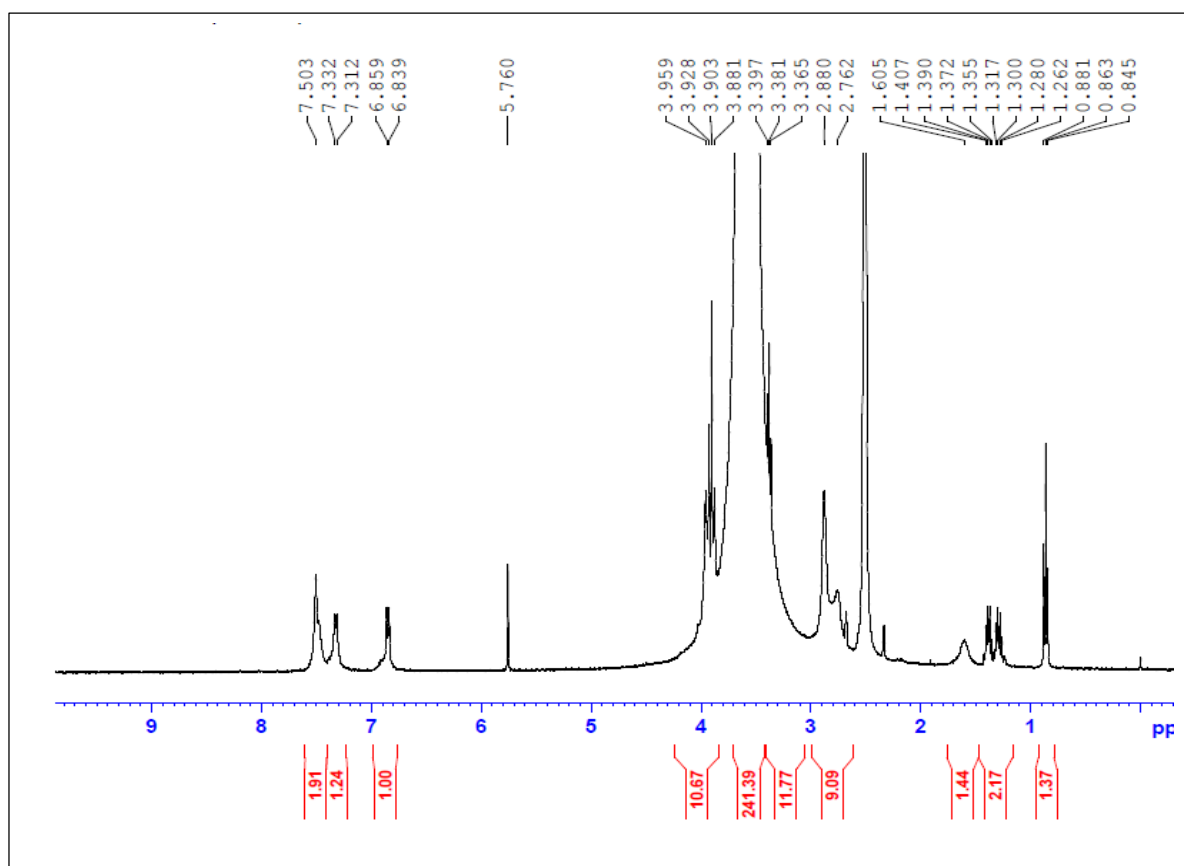
Spectrum 4.12:  $^{13}\text{C}$  NMR spectrum of Hexaminocorand

DMSO- $d_6$

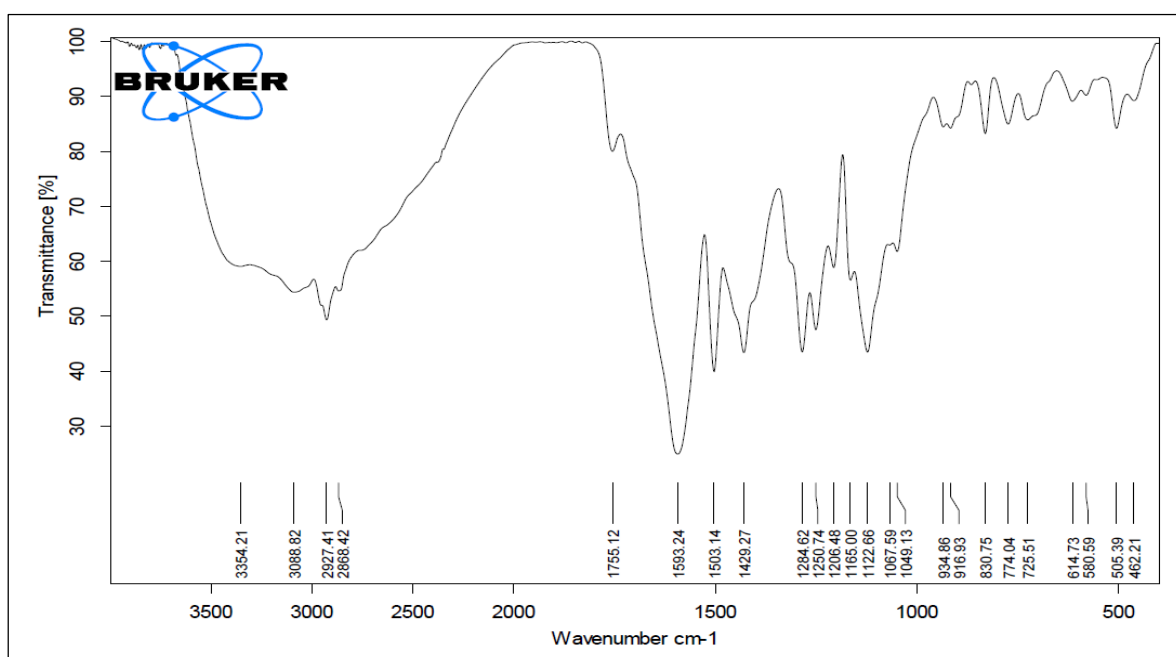


Spectrum 4.13:  $^1\text{H}$  NMR spectrum of pegylatedhexaminocorand

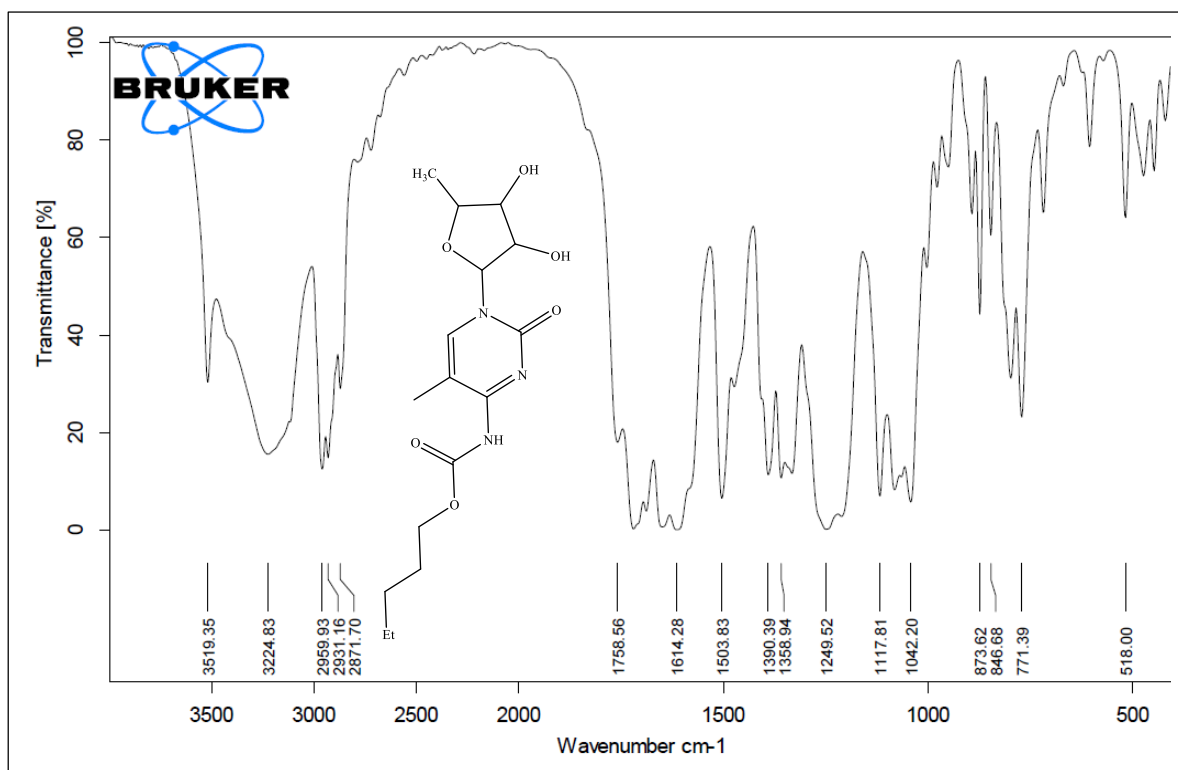
DMSO- $d_6$



Spectrum 4.14: FT-IR spectrum of capecitabine loaded pegylatedhexaminocorand



Spectrum 4.15: FT-IR spectrum of Capecitabine



---

## 4.6. References

- 1 P. Mansfield, A. A. Maudsley, *Phys. Med. Biol.*, 1976, **21**, 847-852.
- 2 R. M. Patten, S. K. Lo, J. J. Phillips, S. C. Bowman, G. M. Glazer, S. D. Wall, J. G. Bova, R. D. Harris, R. L. Wheat, C. D. Jhonson, H. Y. Kressel, A. E. Stillman R. A. Halvorsen, A. A. Moss, *Radiology*, 1993, **189**, 277–283.
- 3 P. Caravan, *Chem. Soc. Rev.*, 2006, **25**, 512-523.
- 4 I. R. Young, D. Ph, G. J. Clarke, M. Sc, D. R. Bailes, M. Sc, F. H. Doyle, G. M. Bydder, *J. Comput. Tomogr.*, 1981, **5**, 543–547.
- 5 M. Yon, C. Billotey, J. Marty, *Int. J. Pharm.*, 2019, **569**, 118577.
- 6 M. Bottrill, L. Kwok, N. J. Long, M. Bottrill, E. Abel, T. Osborne, N. Long, *Chem. Soc. Rev.*, 2006, **35**, 557–571.
- 7 H. Kim, G. H. Lee and Y. Chang, *Future Med. Chem.*, 2018, **10**, 639-661.
- 8 Y. D. Xiao, R. Paudel, J. Liu, C. Ma, Z. S. Zhang, S. K. Zhou, *Int. J. Mol. Med.*, 2016, **38**, 1319–1326.
- 9 A. L. Carrillo, M. Filice, M. J. Guillen, R. Amaro, M. Vinambres, A. Tabero, K. O. Paredes, A. Villanueva, P. Calvo, M. D. P. Morales, M. Marciello, *Mater. Sci. Eng. C*, 2020, **107**, 110262.
- 10 A. Ranga, Y. Agarwal, K. J. Garg, *Indian J. Radiol. Imaging*, 2017, **27**, 141-147.
- 11 T. J. Clough, L. Jiang, K. L. Wong, N. J. Long, *Nat. Commun.*, 2019, **10**, 1–14.
- 12 E. M. Gale, P. Caravan, A. G. Rao, R. J. Mcdonald, M. Winfeld, R. J. Fleck, M. S. Gee, *Pediatr. Radiol.*, 2017, **47**, 507–521.
- 13 D. Xu, S. T. Lu, Y. S. Li, A. Baidya, H. Mei, Y. He, B. Wu, *Drug Des. Devel. Ther.*, 2018, **12**, 3301–3309.
- 14 Y. Jeong, K. Na, *Biomater. Res.*, 2018, **22**, 1–8.
- 15 F. Maghsoudinia, H. A. Zadeh, F. Aminolroayaei, F. F. Birgani, A. Shanei, R. K. Samani *Eur. J. Pharm. Sci.*, 2022, **174**, 106207.

- 
- 16 E. Gallo, C. Diaferia, E. Di Gregorio, G. Morelli, E. Gianolio, A. Accardo, *Pharmaceuticals*, 2020, **13**, 1–15.
  - 17 Z. Yang, H. Lin, J. Huang, A. Li, C. Sun, J. Richmond, J. Gao, *Chem. Commun.*, 2019, **55**, 4546-4549.
  - 18 Y. C. Chen, Q. Ye, T. Gong, J. Kunag, S. Li, *J. Pharm. Biomed. Sci.*, 2018, **8**, 79-83
  - 19 S. A. Sabra, S. A. Sheweita, M. Haroun, D. Ragab, M. A. Eldemellawy, Y. Xia, D. Goodale, A. L. Allan, A. O. Elzoghby, S. Rohani, *J. Pharm. Sci.*, 2019, **108**, 1713–1725
  - 20 E. M. M. Abdelraheem, S. Shaabani, A. Domling, *Synlett.*, 2018, **29**, 1136–1151.
  - 21 A. Mueller, D. F. O. Brien, *Chem. Rev.*, 2002, **102**, 727-757 .
  - 22 D. M. Vriezema, M. C. Aragone, J. A. A. W. Elemans, J. J. L. M. Cornelissen, A. E. Rowan, R. J. M. Nolte, *Chem. Rev.*, 2005, **105**, 1445-1489.
  - 23 D. E. Discher, A. Eisenberg, *Science*, 2002, **297**, 967-973.
  - 24 M. Scarzello, V. Chupin, A. Wagenaar, M. C. A. Stuart, J. B. F. N. Engberts, *Biophys. J.*, 2005, **88**, 2104–2113.
  - 25 D. Jiao, J. Geng, X. J. Loh, D. Das, T. Lee, O. A. Scherman, *Angew. Chem. Int. Ed.*, 2012, **51**, 1-6.
  - 26 P. L. Ahl, L. Chen, W. R. Perkins, S. R. Minchey, L. T. Boni, T. F. Taraschi, A. S. Janoff, *Biochim. Biophys. Acta*, 1994, **1195**, 237–244.
  - 27 F. M. Menger, K. Gabrielson, *J. Am. Chem. Soc.*, 1994, **116**, 1567–1568.
  - 28 T. Dwars, E. Paetzold, G. Oehme, *Angew. Chem. Int. Ed.*, 2005, **44**, 7174–7199.
  - 29 O. Boussif, F. Lezoualch, M. A. Zanta, M. D. Mergny, D. Scherman, B. Demeneix, J. P. Behr, *Pro. Natl. Acad. Sci. USA*, 1995, **92**, 7297–7301.
  - 30 D. S. Guo, K. Wang, Y. X. Wang, Y. Liu, *J. Am. Chem. Soc.*, 2012, **134**, 10244-10250.
  - 31 S. K. M. Nalluri, J. Voskuhl, J. B. Bultema, E. J. Boekema, B. J. Ravoo, *Angew. Chem. Int. Ed.*, 2011, **50**, 9747–9751.
  - 32 T. Ta, A. J. Convertine, C. R. Reyes, P. S. Stayton, T. M. Porter, *Biomacromolecules*,

- 
- 2010, **11**, 1915–1920.
- 33 Q. Duan, Y. Cao, Y. Li, X. Hu, T. Xiao, C. Lin, Y. Pan, L. Wang, *J. Am. Chem. Soc.*, 2013, **135**, 1052-10549 .
- 34 G. Yu, X. Zhou, Z. Zhang, C. Han, Z. Mao, C. Gao, F. Huang, *J. Am. Chem. Soc.*, 2012, **134**, 19489–19497.
- 35 G. Yu, M. Xue, Z. Zhang, J. Li, C. Han, F. Huang, *J. Am. Chem. Soc.*, 2012, **134**, 13248-13251 .
- 36 G. Yu, C. Han, Z. Zhang, J. Chen, X. Yan, B. Zheng, S. Liu, F. Huang, *J. Am. Chem. Soc.*, 2012, **134**, 8711-8717.
- 37 M. Lee, S. Lee, L. H. Jiang, *J. Am. Chem. Soc.*, 2004, **126**, 12724–12725.
- 38 C. Wang, Y. Guo, Y. Wang, H. Xu, X. Zhang, *Chem. Commun.*, 2009, 5380–5382.
- 39 Y. Yao, M. Xue, J. Chen, M. Zhang, F. Huang, *J. Am. Chem. Soc.*, 2012, **134**, 15712-15715.
- 40 G. Saito, J. A. Swanson, K. D. Lee, *Adv. Drug Deliv. Rev.*, 2003, **55**, 199–215.
- 41 X. Zhang, S. Rehm, M. M. S. Sempere, F. Wurthner, *Nat. Chem.*, 2009, **1**, 623–629.
- 42 Y. Zhou, D. Yan, *J. Am. Chem. Soc.*, 2005, **127**, 10468–10469.
- 43 L. A. Erviti, Y. Seow, H. Yin, C. Betts, S. Lakhali, M. J. A. Wood, *Nat. Biotechnol.*, 2011, **29**, 341-345.
- 44 P. G. V. Rhee, R. S. M. Rikken, L. K. E. A. Abdelmohsen, J. C. Maan, R. J. M. Nolte, J. C. M. V. Hest, P. C. M. Christianen, D. A. Wilson, *Nat. Commun.*, 2014, **5**, 5010.
- 45 N. Sakai, S. Matile, *Nat. Chem.*, 2009, **1**, 599-600 .
- 46 T. Shimizu, M. Masuda, H. Minamikawa, *Chem. Rev.*, 2005, **105**, 1401-1443.
- 47 B. Y. Wang, H. Xu, X. Zhang, *Adv. Mater.*, 2009, **21**, 2849–2864.
- 48 C. Wang, Z. Wang, X. Zhang, *Acc. Chem. Res.*, 2012, **45**, 608-618.
- 49 N. Basilio, V. Francisco, L. G. Rio, *Int. J. Mol. Sci.*, 2013, **14**, 3140–3157.

- 
- 50 Q. Pei, X. Hu, L. Wang, S. Liu, X. Jing, Z. Xie, *ACS Appl. Mater. Interfaces*, 2017, **9**, 26740-26748.
- 51 F. Liu, Y. Wang, G. Y. Lu, *Chem. Lett.*, 2005, **34**, 1450–1451.
- 52 Q. Yan, J. Yuan, Z. Cai, Y. Xin, Y. Kang, Y. Yin, *J. Am. Chem. Soc.*, 2010, **132**, 9268–9270.
- 53 W. Tao, Y. Liu, B. Jiang, S. Yu, W. Huang, Y. Zhou, D. Yan, *J. Am. Chem. Soc.*, 2012, **134**, 762-764.
- 54 S. C. Zimmerman, M. S. Wendland, N. A. Rakow, I. Zharov, K. S. Suslick, *Nature*, 2002, **418**, 399–403.
- 55 M. K. Ng, L. Yu, *Angew. Chem. Int. Ed.*, 2002, **41**, 3598-3601.
- 56 H. Jin, Y. Liu, Y. Zheng, W. Huang, Y. Zhou, D. Yan, *Langmuir*, 2012, **28**, 2066–2072.
- 57 Y. Liu, C. Yu, H. Jin, B. Jiang, X. Zhu, Y. Zhou, Z. Lu, D. Yan, *J. Am. Chem. Soc.*, 2013, **135**, 4765-4770 .
- 58 R. Chakrabarty, P. S. Mukherjee, P. J. Stang, *Chem. Rev.*, 2011, **111**, 6810–6918.
- 59 P. Rangadurai, M. R. Molla, M. Caissy, S. Thayumanavan, *J. Am. Chem. Soc.*, 2016, **138**, 7508-7511.
- 60 S. Dong, Y. Luo, X. Yan, B. Zheng, X. Ding, Y. Yu, Z. Ma, Q. Zhao, *Angew. Chem. Int. Ed.*, 2011, **50**, 1905–1909.
- 61 B. Zheng, F. Wang, S. Dong, F. Huang, *Chem. Soc. Rev.*, 2012, **41**, 1621-1636.
- 62 E. M. M. D. Valle, *Process Biochem.*, 2004, **39**, 1033–1046.
- 63 X. Chi, H. Zhang, G. I. Vargas-zu, G. M. Peters, J. L. Sessler, *J. Am. Chem. Soc.*, 2016, **138**, 5829-5832.
- 64 K. Chen, Y. S. Kang, Y. Zhao, J. M. Yang, Y. Lu, W. Y. Sun, *J. Am. Chem. Soc.*, 2014, **136**, 16744-16747.
- 65 K. Kim, *Chem. Soc. Rev.*, 2002, **31**, 96–107.
- 66 X. Liu, K. Jia, Y. Wang, W. Shao, C. Yao, L. Peng, D. Zhang, X. Y. Hu, L. Wang, *ACS*

- 
- Appl. Mater. Interfaces*, 2017, **9**, 4843-4850.
- 67 J. Zhou, M. Chen, G. Diao, *ACS Appl. Mater. Interfaces*, 2014, **6**, 18538-18542.
- 68 L. B. Meng, W. Zhang, D. Li, Y. Li, X. Y. Hu, L. Wang, G. Li, *Chem. Commun.*, 2015, **51**, 14381-14384.
- 69 R. Muzzalupo, F. P. Nicoletta, S. Trombino, R. Cassano, F. Iemma, N. Picci, *Colloid. Surf. B Biointerfaces*, 2007, **58**, 197–202.
- 70 D. B. Mahmoud, S. A. Afifi, N. S. E. Sayed, *Mol. Pharmaceutics*, 2020, **17**, 3952-3965.
- 71 J. Wang, T. Wang, X. Liu, Y. Lu, J. Geng, *RSC ADV.*, 2020, **10**, 18572–18580.
- 72 V. K. Ahire, D. D. Malkhede, *J. Indian Chem. Soc.*, 2023, **100**, 100880.
- 73 H. Peng, B. Xie, X. Yang, J. Dai, G. Wei, Y. He, *Chem. Commun.*, 2020, **56**, 8115-8118.
- 74 U. Rehman, R. M. Sarfraz, A. Mahmood, Z Hussain, H. E. Thu, N. Zafar, M. U. Ashraf, N. Batool, *Curr. Drug Deliv.*, 2021, **18**, 1256-1271.